Karinh Emma Josephina Eurenius

Proton Conductivity in Acceptor-Doped Lanthanide Based Pyrochlore Oxides

Faculty of Science

2009

ISBN 978-91-628-7897-9

Proton Conductivity in Acceptor-Doped Lanthanide Based Pyrochlore Oxides

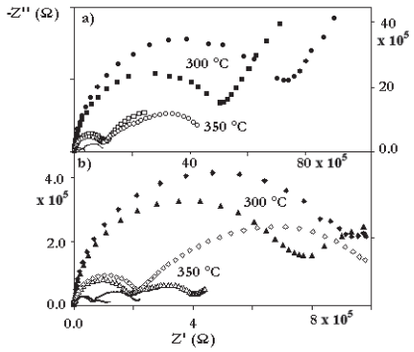

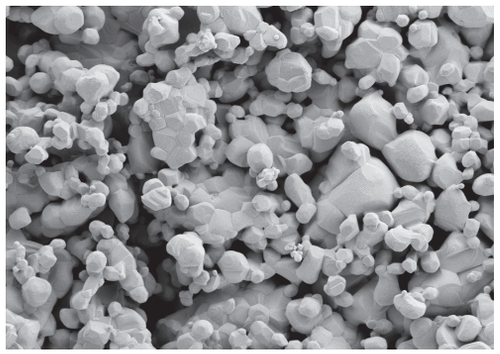

Karinh Emma Josephina Eurenius

Ph.D. thesis
Department of Chemistry
University of Gothenburg

UNIVERSITY OF GOTHENBURG

THESIS FOR THE DEGREE OF DOCTOR OF PHILOSOPHY

Proton conductivity in acceptor-doped lanthanide based pyrochlore oxides

Karinh Emma Josephina Eurenius

Inorganic Chemistry
Department of Chemistry

GÖTEBORGS UNIVERSITET

University of Gothenburg
Gothenburg, Sweden 2009

Proton conductivity in acceptor-doped lanthanide based pyrochlore oxides

Karinh Emma Josephina Eurenius

ISBN: 978-91-628-7897-9

Doktorsavhandlingar vid Göteborgs Universitet

Department of Chemistry
University of Gothenburg
SE-412 96 Gothenburg
Sweden
Telephone: +46 (0)31 772 1000
eureniuk@chem.gu.se

Printed at Chalmers Reproservice AB
Göteborg, Sweden, 2009

Till min man Jonas, mamma Ingrid och mormor Gunvor

”Blott en dag, ett ögonblick i sänder”

Abstract:

A high interest in developing new materials for SOFC applications in the temperature range of approximately 200–500 °C has been growing lately. The lower activation energies for proton (H^+) mobility can give higher conductivity in this temperature range. A demand on finding new H^+ conducting materials as electrolytes in fuel cells is thereby the result. The materials should preferably have high H^+ concentration and mobility, be chemically stable at the required operating temperatures and be electronically insulating. Although structure-types other than the well known perovskites, such as pyrochlores, have been of interest as novel materials for protonic devices, significantly less research has been carried out on these systems. This makes further detailed investigation of proton conduction in pyrochlores an important step on the way to finding the next family of materials for proton conducting applications.

This thesis presents the synthesis and characterization of the structure and conductivity of several pyrochlore oxide compounds. The synthesis for all the studies was concentrated on traditional solid state sintering, while characterization have been conducted with X-ray diffraction (XRD), thermogravimetric analysis (TGA), infrared spectroscopy (IR), scanning electron microscopy (SEM) and electrochemical impedance spectroscopy (EIS). Determination of particle size distribution (PSD), calculations of transport numbers via the electromotive force method (EMF) and EIS in a controllable gas cell for the $Sm_{2-x}Ca_xTi_2O_{7-x/2}$ material were carried out (Paper IV).

The proton conductivity in pyrochlore materials has been examined for several acceptor doped compounds, such as $A_{2-x}Ca_xB_2O_{7-x/2}$ (A = La, Sm, Yb; B = Ti, Sn, Zr, Ce) and $A_2B_{2-x}Y_xO_{7-x/2}$ (A = Sm; B = Ti, Sn). The materials exhibit high purity and chemical stability. The effects of A- and B-site doping, the significance of the B-site ion, and the importance of the lanthanide size at the A-site were all studied in relation to their impact on proton conductivity.

Expansions or reductions of the cell depending on doping site or choice of A- and B-site ions were confirmed by 2θ-shifts in the XRD patterns. TGA gave affirmative results regarding the loss of protons from the hydrated samples at expected temperatures. The results were linked with IR spectra confirming peaks at characteristic positions for O-H stretch vibrations as well as a isotopic shifts for samples treated under heavy water.

The EIS measurements showed overall elevated conductivities under wet gas conditions and isotope effects with deuterated water. The A-site doped samples showed close to one order of magnitude higher conductivities compared to the B-site doped samples. Varying the B-site ion with increasing ionic radius (Ti, Sn, Zr, Ce) showed higher proton conductivity levels for the B-site ions with smaller ionic radii and higher electronegativity. Further, the effect of the lanthanide contraction on proton conduction could be seen through varying the A-site constituent along the lanthanide group. The EMF and the EIS measurements carried out under controlled gas atmospheres gave transport numbers supporting dominant proton conductivity in $Sm_{1.92}Ca_{0.08}Ti_2O_{7-\delta}$. Large electrode polarization resistances were noted for all temperatures and gas concentrations. The Gorelov method was used for correction.

This work provides a wider understanding of the influence of the doping site, choice of A and B-site ions and microstructure on proton conduction in pyrochlore systems.

Key words: Pyrochlore, Rietveld refinement, Proton conductivity, Electrical impedance spectroscopy, Concentration Cell Electromotive Force Method.

List of publications

The thesis was based on the following papers:

Articles

I. Investigation of Proton Conductivity in $Sm_{1.92}Ca_{0.08}Ti_2O_{7-\delta}$ and $Sm_2Ti_{1.92}Y_{0.08}O_{7-\delta}$ Pyrochlores
K.E.J. Eurenius, E. Ahlberg, I. Ahmed, S.G. Eriksson and C.S. Knee[*]
Solid State Ionics (2009), doi:10.1016/j.ssi.2009.05.004

II. Proton Conductivity in $Sm_2Sn_2O_7$ Pyrochlores
K.E.J. Eurenius[a, *], E. Ahlberg[a] and C.S. Knee[a]
Submitted to Solid State Ionics (2009)

III. Proton conductivity in $Ln_{2-X}Ca_XSn_2O_{7-\delta}$ (Ln = La, Sm, Yb) pyrochlores as a function of lanthanide size
K.E.J. Eurenius[a, *], E. Ahlberg[a], S.G. Eriksson[b] and C.S. Knee[a]
Submitted to Solid State Ionics (2009)

Manuscripts

IV. Proton Conductivity in the $Sm_{1.92}Ca_{0.08}Ti_2O_{7-\delta}$ Pyrochlore Structure with the Concentration Cell Electromotive Force Method and Electrochemical Impedance Spectroscopy
K.E.J. Eurenius[a, *], H. Bentzer[b], N. Bonanos[b], E. Ahlberg[a], S.G. Eriksson[c] J. Phair[b] and C.S. Knee[a]

V. Protonic conduction in $Sm_{1.92}Ca_{0.08}B_2O_{7-\delta}$ (B = Ti, Sn, Zr and Ce) pyrochlores and C-type compounds
K.E.J. Eurenius[a, *], E. Ahlberg[a], S.G. Eriksson[b] and C.S. Knee[a]

Specification of my contribution to the appended papers

I have synthesized, characterized and analysed the samples in all the studies. Rietveld analysis has been carried out by Dr. C. S. Knee. I have been co-author of the papers where the papers were written jointly with Dr. C. S. Knee and Prof. E. Ahlberg. Paper IV was written partly together with PhD. H. Bentzer and Prof. N. Bonanos.

TABLE OF CONTENTS

1 Introduction

1.1 Fuel Cells and Proton Mobility

A vital component of the hydrogen economy is a fuel cell in which hydrogen and oxygen gases are combined to produce water and electricity. Compared with established power sources many fuel cells offer remarkable efficiencies (typically 60 %), to produce direct current (DC) and can be viewed as a clean source of energy.

An examples of such a cell, is the solid oxide fuel cell (SOFCs). This is suitable for both medium (vehicles, field units) and large scale (power stations) power generation applications (Fig. 1).

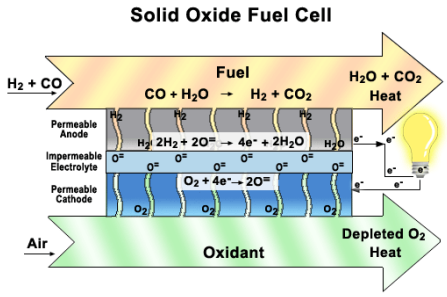

Figure 1. A Solid Oxide Fuel Cell (SOFC).[1]

The significant, and so far unresolved, problem associated with SOFCs based on current state-of-the-art oxide ion conducting elektrolytes, is the high temperature (> 800 °C) of operation[2]. This is to overcome the activation energy of oxide ion conduction which severely limits the uses of SOFCs.

Based on this background there is a high interest in the progress of new materials for SOFC applications in the so called "intermediate" temperature range (approximately 200–500 °C). The lower activation energies associated with proton (H^+) mobility give higher conductivity in this temperature range. A strong interest in new H^+ conducting materials as electrolytes in fuel cells has hence been the result.

Some basic desirable properties for a proton solid electrolyte include high H^+ concentration and mobility. They should further be chemically stable at the required operating temperatures. In addition, they ought to exhibit insulating or be very poor electrical conductors, since the only mobile species should be H^+.

1.2 Novel materials

The search for high temperature proton conductors has mainly been focused on perovskites[3,4,5]. Materials with the pyrochlore structure have also been considered as candidates for high and medium temperature proton conducting applications[6]. However, significantly less work has been done on pyrochloes and this makes the area rich with potential from both an experimental and

theoretical viewpoint. A systematic examination of acceptor doped pyrochlore systems as proton conductors would thereby be an important contribution to the scientific society.

1.3 Aim

The intent with this study is to find suitable materials for proton conductivity in pyrochlores where the aim has been to find phase pure pyrochlore oxides which are chemically stable. Unanswered questions regarding A-site substitution/deficiency in comparison to B-site substitution/deficiency to clarify the effect on H^+ conductivity (Paper I and II) was one of the first aims.

Further, the effect of the lanthanide contraction (paper III) on the conductivity in A-site acceptor doped systems with the same nominal level of oxygen vacancies was investigated.

The transport numbers of ($Sm_{1.92}Ca_{0.08}Ti_2O_{6.96}$) was looked at in detail and conductivity studies were carried out on the same material under controlled partial pressure (Paper IV). The results showed that the transport numbers typically responded to values for ionic conduction.

To limit electronic conduction, B-site ions with empty valence shells such as $Nb^{5+}/Ta^{5+}/Ti^{4+}/Zr^{4+}$, are preferable candidates for possible proton conductors. Further, the effect of the electronegativity of the B-site ion on the proton conduction was explored (Paper V). The study carried out was for finding trends with regards to proton conductivity combined with structural analysis and proton uptake. Correlation with ionic size of the B-site ion showed to be highly relevant and the samples with the smallest cell parameters also gave the highest proton conduction.

Experimental conditions required for proton absorption and investigations of proton conductivity as function of temperature and atmosphere were necessities for all the studies in this project.

2 Background

2.1 Fundamental approach

Extensive studies of various perovskite oxides have been reported for several decades[7]. Examples such as $SrCeO_3$ and $BaCeO_3$ [2] have shown high and pure proton conductivity. A summary of oxide materials and their proton conduction can be seen in Figure 2.

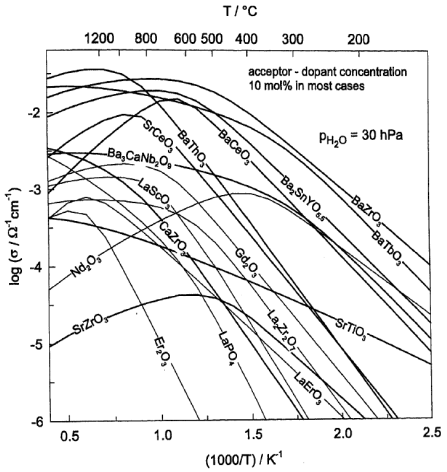

Figure 2. Kreuer's summary[2] of proton conductivities of oxide systems; the figure is based on concentrations and mobilities calculated by Norby and Larring[8].

Studies of proton mobility in pyrochlore oxide systems have been concentrating on acceptor doped derivatives of $La_2Zr_2O_7$[9]. The investigations have so far included recordings of infrared (IR) spectra[10,11] and EIS measurements[12,13]. Very recently, quantum mechanical simulation techniques have been employed with oxide ion conducting electrolytes. The aim of the study was to improve the understanding of the local proton environment and the details of the migration processes in $La_2Zr_2O_7$[14].

Pyrochlores typically show 1-2 orders of magnitude lower conductivities than the best performing perovskites in the intermediate temperature range (200 - 550 °C). This temperature 'gap' has in particular been reported by Norby[15] (Fig. 3). Finding materials operating in this range and hence narrowing it would be beneficial for manufacturing technological equipment which needs to function in this temperature span.

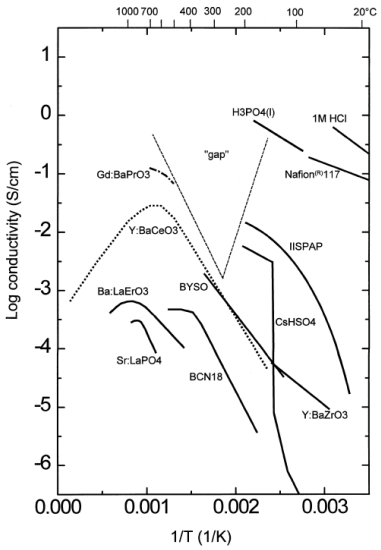

Figure 3. Norby's study[15] of proton conductivity as a function of temperature from selected compounds in the literature[16,17].

2.2 Technological approach

Traditional solid oxide fuel cells (SOFC) have so far been preferred due to robustness[18] compared to aqueous electrolyte cells based on phosphoric acids or alkaline materials. The common high temperature (>800 °C) SOFC has several flaws such as low efficiency, long start up times, high temperature corrosion and demanding thermal insulation[19,20].

In general, operating fuel cells at lower temperatures, will overcome many of the problems which are currently experienced regarding high temperature cells. A typical fuel cell based on a proton conducting electrolyte can be viewed in Figure 4 below.

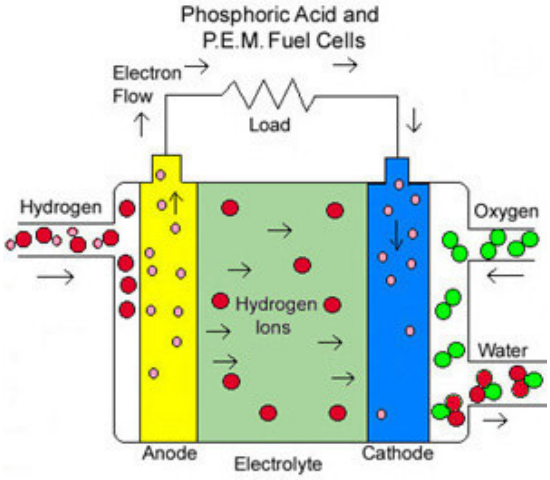

Figure 4. Schematic of how a phosphoric and Proton Exchange Membrane fuel cell operate[21].

A perfluorosulphonic polymer material, known as Nafion, has proven to be a typically useful electrolyte in low temperature polymer membrane electrolyte fuel cells. However, the problems regarding operating in the low temperature range are the requirement for expensive platinum catalysts and high purity fuel. The cells further encounter difficulties with low electrical efficiency issues, which are typically 30 – 45%.[2]

Extensive research has been carried out towards finding suitable materials for all parts of the fuel cell, where a proton conducting electrolyte is of high priority. Kreuer[2] and Norby[15] have, amongst others, carried out reviews on the results so far on novel materials. They both point out the lack of suitable compounds in the intermediate temperature range.

The main problems are the stability of the compound in combination with low proton conduction. Most stable compounds such as perovskite rare-earth oxides[22] give low proton conductivity, while highly conductive samples, as cerate perovskites[23], are unstable. Further, the ability to model and fully understand the quantum mechanical proton transfer process is highly complex.[15]

2.3 Structural aspects

It has been seen that distortions from cubicity in perovskite-related oxides decrease the proton mobility[24]. Islam et al[25] reported on cubic $BaZrO_3$ where trapping effects from the dopants were studied in direct correlation to the ionic radius of the dopant. The smaller the dopant the higher the binding energy and the magnitude of association for hydroxyl-dopant pairs increase along $Y^{3+} < Yb^{3+} < In^{3+} < Sc^{3+}$.

Iwahara *et al.*[26] showed that the proton conductivity for the same system increased with increasing ionic radius of the B-site cation dopant as far to Y^{3+}, and then decreased for the larger lanthanides (Nd^{3+}).

Previous studies on the trapping behaviour of protons[27] have suggested that accumulation of valence charge on the oxygen atoms would strengthen the O-H bonds. This would hence increase the energy migration barriers and the mobility of the protons would decrease. However, Wahnström *et al.*[28] then reported on the transfer of charge from the dopants to the oxygen host lattice were distributed rather homogeneously over long distances. It was found that the ability to form a strong hydrogen bond with the next nearest oxygen was the most important factor for stabilizing protons in the vicinity of dopants. Hence, the smallest dopants in the study (Ga and Sc) allowed the largest OH tilting which gave the shortest H-O bonds, and the most stable proton sites were found here.

Haugsrud and Norby[29] studied Ca-doped rare-earth niobate series, $RE_{1-x}Ca_xNbO_4$ (RE=La, Nd, Gd, Tb, Er, Y; x=0.01–0.05). Conductivity was here clearly dominated by protons and the total and partial protonic conductivity decreased with decreasing radius of the rare-earth cations (La > Nd > Tb > Er). It was explained by the general decrease in polarizability of the proton-hosting oxide ion sublattice, giving a smaller and more rigid lattice overall. Therefore, even if the oxygen ions are closer on average, the lattice is not as flexible and a proton transfer becomes harder and the proton conductivity decreases. Further, the hydration became more exothermic with the lanthanide contraction, agreeing with binary rare-earth oxides (RE_2O_3)[30]. However, in rare-earth phosphates ($REPO_4$)[31] the trend is the opposite and the same is the case for the pyrochlores in this study.

3 Overview of solid state proton conductors

3.1 Proton conductors

Proton conducting materials are important from both academic and technological angles and have been studied from many points of view. Proton transport is the answer to many problems in a range of different technological devices and the academic interest of understanding the proton transport are directed towards structural and physical properties of the materials.

Some of the most important discoveries from the 20th century may be attributed to Mollow[32], who reported on electrical properties of zinc oxide. Further, Rudolph[33] stated that protons were positive charge carriers and Pope and Simkovich[34] reported on protonic species in perovskite oxides.

3.1.1 Perovskites

In 1980, Takahasi and Iwahara[35] related the electrical properties of $LaYO_3$ and $SrZrO_3$ with incorporated water vapour in the structure. This opened a door for characterization of proton conducting perovskite materials by various experimental and theoretical techniques. The $SrCeO_3$ and $BaCeO_3$ systems[2] were the first oxides to show high levels of proton conductivity (10^2 – 10^{-3} Scm^{-1}, 600 – 1000 °C).

Many perovskites, *e.g.*, Y-doped $BaCeO_3$[36] and $Ba_3Ca_{1.18}Nb_{1.82}O_{8.73}$ (BCN-18)[37] display a combination of high proton mobility and relatively high proton concentrations. This has lead to proton conductivities of close to 10^{-3} S cm^{-1}.

3.1.2 Pyrochlores

The study by Shimura *et al.*[38] in 1996, reports on the ionic, and in particular the proton, conductivity of a number of rare earth pyrochlore-type oxides of the form $Ln_2Zr_{2-x}Y_xO_{7-\delta}$ and $Y_2Ti_{2-x}M_xO_{7-\delta}$ (M = In and Mg; Ln = La, Nd, Sm, Gd and Er). The $Ln_2Zr_{1.8}Y_{0.2}O_{7-\delta}$ systems were found to have conductivities comparable to perovskite systems under hydrogen containing atmospheres at T ≥ 600 °C. No clear indication of proton conduction in the $Y_2Ti_{2-x}M_xO_{7-\delta}$ systems were found. The importance of introducing oxygen vacancies for the proton conduction properties of the $Ln_2Zr_{1.8}Y_{0.2}O_{7-\delta}$ materials can be viewed in Figure 5, where the doped and undoped systems show high and low conductivities respectively.

Further investigations on substituted $La_2Zr_2O_7$ systems have been reported by Omata and co-workers[39],[40]. In these studies, the electrical conductivity of Ca^{2+}- doped samples of the form $(La_{2-x}Ca_x)Zr_2O_{7-\delta}$ (x = 0.015, 0.03, 0.05) and $La_2(Zr_{2-x}Ca_x)O_{7-\delta}$ (x = 0.015) were investigated. This work allows the effect of oxygen vacancies, introduced through substitution at both the A- and B-site of the pyrochlore structure, to be investigated. It is highly relevant to the results presented in papers I and II.

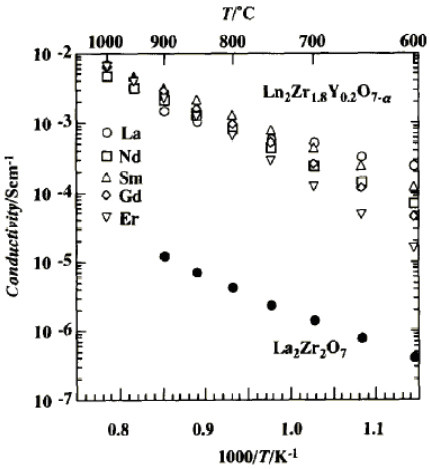

Figure 5. Conductivities of $La_2Zr_2O_7$ and $Ln_2Zr_{1.8}Y_{0.2}O_{7-\delta}$ (Ln= La, Nd, Sm, Gd and Er) in hydrogen saturated with water vapour.[38]

Omata *et al.*. found that under wet hydrogen conditions at 600 °C the A-site doped system $(La_{2-x}Ca_x)Zr_2O_{7-\delta}$ gave better proton conduction than the B-site substituted system. The samples have the same number of oxygen vacancies (δ = 0.015), while $(La_{1.97}Ca_{0.03})Zr_2O_{7-\delta}$ showed a conductivity of 3.9×10^{-2} S m^{-1} and $La_2(Zr_{1.985}Ca_{0.015})O_{7-\delta}$, $\sigma = 1.0 \times 10^{-2}$ S m^{-1}. This trend was attributed to the greater H^+ dissolution in the A-site doped materials, which in turn was suggested to be linked to the presence of different oxygen vacancy sites in the structures. In general, a high level of oxygen deficiency is desirable as these systems have the potential to incorporate large numbers of protons. It should be noted that the substitution levels achieved in $La_2Zr_2O_7$ are very low, *e.g.* x = 0.05 is the maximum for $(La_{2-x}Ca_x)Zr_2O_{7-\delta}$. This limits the number of protons to $(La_{1.95}Ca_{0.05})Zr_2O_{6.95}(OH_2)_{0.05}$ per formula unit, if assuming full protonation can be achieved. Higher proton concentrations are theoretically achievable in oxygen deficient pyrochlores.

Haugsrud and Norby have studied the mixed ionic-electronic conductor behaviour of $La_{1.98}Ca_{0.02}Ti_2O_{7-\delta}$[41]. It should be noted that this phase has a significant orthorhombic distortion from the ideal cubic pyrochlore structure. EMF measurements in wet hydrogen revealed a small protonic contribution to the total conductivity ($\sigma_{prot} \approx 6 \times 10^{-5}$ S cm^{-1} at 750 °C) that was otherwise dominated by electronic conductivity.

Further, Petric et al[42] showed that pyrochlore solid solutions of $Y_{3+x}Ta_{0-x}O_{7-x}$ exhibited proton conductivities which increased with increasing x up to x=0.2. This effect was explained on the basis of the increased disorder of the oxygen vacancies. The materials were found to be proton conductors up to ~400 °C.

Recently, studies show that systems such as $Er_2Ca_{0.04}Ti_2O_{7-\delta}$ exhibit amorphous phases where oxygen vacancies were found to be the most important charge carriers in the grain interior, while proton mobility was highly represented in the grain boundaries[43].

3.1.3 Fluorite and C-type structures

Fluorite type structures, such as $La_xWO_{3+1.5x}$ ($x \approx 6$)[44], $(Ln_{1-x}Ln'_x)_2Zr_2O_7$[45] and $Ce_{0.8}M_{0.2}O_{2-\delta}$ (M = La, Y, Gd, Sm)[46], are similar to pyrochlores. The latter have been found to have high proton

conductivities (~10^{-2} - 10^{-3} S cm^{-1} at 650 - 900 °C), while other fluorites have shown considerably lower values[47,48].

Further, compounds such as $Sm_2Ce_2O_7$[49], melts of Ta_2O_5-Y_2O_3[50] and $Gd_{1-x}Ce_xO_{1.5+x/2}$[51] have been investigated and found to exhibit a superstructure denoted C-type phase (*Ia3*, Z = 16). It is derived from a fluorite structure with regards to the ordering of the oxygen vacancies, but no proton conductivities have been reported. In paper V, the $Sm_{1.92}Ca_{0.08}Ce_2O_{6.96}$ compound, which exhibits a C-type structure related to the fluorite structure, is part of the study.

3.2 The Lanthanide Group

Several of the oxides of the lanthanide elements (Z = 58 - 71) exhibit preferences for forming pyrochlore structures. Lanthanides can in addition be used in open laboratory environments they are relatively cheap, stable oxides and are the largest naturally occurring group in the periodic table. The name 'lanthanoid' or 'lanthanon' can also be for the group, where the Swedish scientist Cronstedt (1791), was the first to report that he had discovered a new heavy mineral. Further, his Swedish collegue Berzelius (1803) together with Claproth and Hisinger, isolated the same mineral or oxide (earth) and named it Ceria after asteroid Ceres. Later, their country man Mosander (1839 – 1843) showed that Ceria was a mixture of elements and in 1907 the oxides of La, Y, Sc and 13 other lanthanides were isolated in Ytterby. This is celebrated in four out of the thirteen lanthanide names i.e. Yttrium , Terbium, Erbium and Ytterbium; also Scandium, Holmium and Thulium come from Sweden where the names refer to Scandinavia, Stockholm and 'the northern land' Thule[52].

An interesting feature of the lanthanides is the so called Lanthanide contraction. The lanthanides start to fill the f-orbitals, which have a low shielding effect. As the number of protons in the atom nucleus increases with the atomic number, the electrons are more attracted to the nucleus and therefore the atom radius decreases[53].

Studies on lanthanide containing oxides and the contraction effects on conductivity have previously been carried out by Norby[54] and Haugsrud[55]. Norby *et al.* studied the conductivity contributions from protons, native ions, and electrons in cubic systems Y_2O_3+ 1 mol% MgO and Sm_2O_3 , Gd_2O_3 and YYb_2O_3 +1-5 mol% CaO. All systems gave dominant proton conductivities in wet atmospheres and reduced temperatures, where the oxides dissolve protons to compensate for the acceptor doping.

Furthermore, proton conducting oxides based on lanthanides may offer greater chemical stability in comparison to systems based on alkaline earths such as Ba or Sr.

3.3 Pyrochlore oxides

The ideal structure of a stochiometric $A_2B_2O_7$ pyrochlore is shown below (Fig 6). A is generally the larger ion and B the smaller and the pyrochlore structure has a typical cell parameter of ~10 Å.

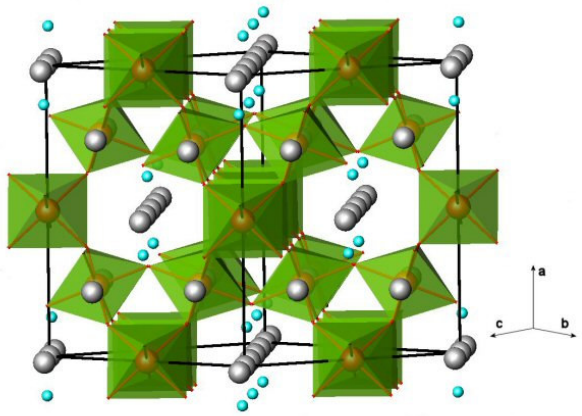

Figure 6. The pyrochlore structure with rings of BO_6 octahedra in green, A cations in grey and non-polyhedral oxygens in cyan.[56]

The pyrochlore structure can be viewed of as a 3-D framework of interlinked BO_6 octahedra that possess channels running along the 110 crystal direction in which the A cations are located. An important feature of the structure is the presence of two distinct oxygen sites. It is the O(1) oxygen which bonds to the B sites only and makes up 6 of the 7 oxygens in the formula unit. Further, the non-framework O(2) oxygen that bonds to the A sites and form zig-zag chains inside the channels[57].

To describe the symmetry of the crystal, space groups are used and pyrochlores belong to the cubic *Fd-3m* space group. The atomic coordinates specify the 3D dimensional structure of the system and give the position of the atoms in the structure as x, y and z coordinates. These are often described with Wyckoff positions. A Wyckoff position is a point belonging to a set of points for which site symmetry groups are subgroups of the space group[58]. The number in the Wyckoff site symmetry indicates how many atoms there are of, for instance, kind A (16) in the unit cell. The following letter defines the relationship between the atoms and implies the total number of equivalent points.[59] The atomic coordinates and the Wyckoff positions for a pyrochlore structure can be seen in the table below.

	x	y	z	Wyckoff site symmetry
A	$^1/_2$	$^1/_2$	$^1/_2$	16d
B	0	0	0	16c
O(1)	x [a]	$^1/_8$	$^1/_8$	48f
O(2)	$^3/_8$	$^3/_8$	$^3/_8$	8b

[a] x~0.3

Table 1. The atomic coordinates and the Wyckoff positions for a pyrochlore structure, *Fd-3m* space group. [60]

In some respects the 3D channels running through the material (Figure 6) suggest that these compounds should intrinsically have better conductivity properties than perovskites, and certain pyrochlores do show good oxide ion mobility as discussed[61].

Various studies have dealt with finding novel materials and gaining pure phases by studying the reactants' properties and combining them with extensive structural work. In osmium oxides[62], binary systems such as $Sm_2Ti_2O_7$-$MTiO_3$ (M = Mg, Co, Ni)[63] and $Gd_{1.82}Cs_{0.18}Ti_2O_{6.82}$[64], the compounds crystallizes in general in cubic pyrochlore structures. Amarilla *et al.* reported on pyrochlore-type structured materials such as $M_2(GeTe)O_6$ (M = K, Rb, Cs)[65] and Kumar *et al.*[66] investigated Mg_2MTaO_6 (M = Nd, La), which are typical defective cubic pyrochlore structures. Kennedy *et al.* investigated pyrochlore stannates and their structural and bonding trends[67]. Shlyakhtina et al examined the relation between Ca-doping of $Yb_2Ti_2O_7$ and the electrical conductivity of the oxide ions. It was found that the dopant successfully resided on the Yb-site via neutron diffraction studies and that the material would be suitable for high temperature proton devices[68].

Tuller[69] investigated a range of fluorites and pyrochlores such as $Gd_2(Zr_xTi_{1-x})_2O_7$ which concentrated on mixed ionic conduction (oxygen ion) of electrode materials.

The stability of pyrochlores can be predicted from the tolerance factor (t_f) and is described via the ionic radius (i.r.) of the A- and B-site ion in the pyrochlore structure ($A_2B_2O_7$) according to Equation 2:

$$t_f = \frac{i.r._{A-ion}}{i.r._{B-ion}} \qquad \text{Equation 2}$$

The t_f for pyrochlores from the lanthanide family is in general much larger ($1.5 < t_f < 1.9$) than the one for typical perovskites ($0.9 < t_f < 1.0$)[70]. The latter is dependent on the ionic radii of oxygen according to Equation 3:

$$t_f = \frac{IR_{A-ion} + IR_{O-ion}}{\sqrt{2(IR_{B-ion} + IR_{O-ion})}} \qquad \text{Equation 3}$$

The above is discussed in paper V, where a trend can be seen towards smaller values of t_f for pyrochlores giving higher proton conductivities.

3.4 Defect chemistry

In defect chemistry, the perfect crystal lattice is one where all atoms rest on specific lattice positions. This can only be hypothetically obtained at 0 K, where theoretically no vibrations occur. In reality, no crystals are perfect and the defects the crystals have under normal conditions are of great importance for obtaining an understanding of the material studied. The defects are commonly divided into two classes: the stochiometric and the non-stochiometric defects[71].

3.4.1 Defects in stochiometric compounds

If a charged point defect is formed in a stoichiometric crystal, a complimentary point defect with opposite effective charge must be formed to conserve the electroneutrality. Two types of defect structures have been found to be important in stoichiometric metal oxides. These are termed Schottky and Frenkel defects, respectively, honouring early contributions of two of the many

German scientists who pioneered the development of defect chemistry (Schottky (1935), Frenkel (1926))[72].

3.4.1.1 Schottky disorder

A stoichiometric crystal with Schottky disorder (Fig. 7) contains equivalent concentrations of cation and anion vacancies. Schottky defects can only occur at outer and inner surfaces or dislocations and will diffuse into the crystal until equilibrium is reached.

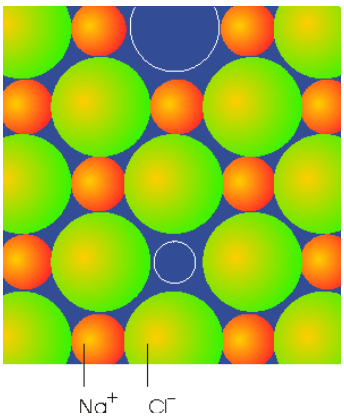

Figure 7. Schematic of a Schottky disorder in a NaCl lattice.[53]

3.4.1.2 Frenkel disorder

A stoichiometric crystal with Frenkel disorder (Fig. 8) contains the same concentrations of metal vacancies and metal interstitial ions. The Frenkel disorder forms when an ion in the lattice moves to an interstitial site. Contrary to the Schottky defects, Frenkel defect pairs can be formed directly inside the crystal.

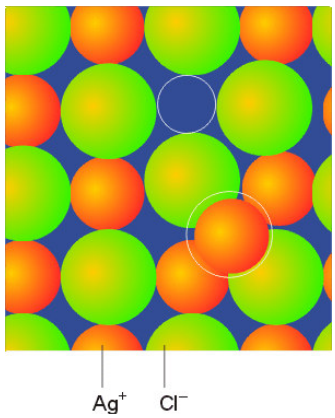

Figure 8. Schematic of a Schottky disorder in a AgCl lattice.[53]

Although Schottky and Frenkel disorder may be simultaneously present in stoichiometric compounds, one type of disorder usually predominates. As a rough rule Schottky disorder is

favoured in crystals where the cations and anions are of comparable size, while Frenkel disorder predominates when the sizes of the cations and anions are appreciably different. Another factor is that Schottky disorder tends to dominate when the structure is very effectively packed so that the interstitials that are part of Frenkel pairs are hard to form.[72]

Studies on spontaneous cationic Frenkel pair recombinations in the pyrochlore $La_2Zr_2O_7$ show a complex behaviour. The disorder is dependent on the distance between the vacancy and the interstitial and the nature of the cation lying in between them. In general it was seen that the recombinations increase with temperature[73].

3.4.2 Defects in non-stochiometric compounds

Non-stochiometry can be introduced via doping of the material in question, which commonly is known as an extrinsic defect. The dopants can occupy an interstitial site or substitute for atoms in the host lattice. In this study the materials have been doped with other atoms of lower valancy in order to create oxygen vacancies (Papers I - V).

In the development of the field of defect chemistry of inorganic compounds various systems of notation have been proposed and used to describe point defects. However, the most widely adopted system is that due to Kröger and Vink [74]. This system describes crystals in terms of structural elements, and an imperfection is indicated by a major symbol with sub- and superscripts. The species involved is represented using the standard element symbols (e.g. oxygen: O, samarium: Sm), with 'V' indicating a vacancy. The superscript gives the effective charge of the defect, i.e. the charge of the defect compared to the charge of the normal expected species on the crystal lattice. The subscript indicates which site the defect occupies. A point, '•', is used for net positive charge, '´' for net negative charge and 'x' for zero net charge, with 'i' indicating an interstitial site. For further explanations see Equations 7 – 9.

3.5 Conductivity of protonic defects

The proton conductivity (σ_{H+}, S cm^{-1}) is described by the product of the charge (zF: z, no unit; F, As mol^{-1}), the concentration of the charge carriers (C, mol cm^{-3}) and the mobility of the charge carriers (μ, cm^2 s^{-1} V^{-1}) as follows (Eq. 4):

$$\sigma_{H+} = zF \cdot C_{H+} \cdot \mu_{H+} \qquad \text{Equation 4}$$

The mobility can be described by the Nernst-Einstein relation i.e. the diffusivity (D, cm^2 s^{-1}), the gas constant (R, J mol^{-1} K^{-1}), the absolute temperature (T, K), the Faraday constant (F, C mol^{-1}) and the number of charges (z, no unit) as follows (Eq. 5):

$$\mu_{H+} = \frac{zFD}{RT} \qquad \text{Equation 5}$$

In ideal circumstances, the mobility and diffusivity is not dependent on the concentration of protons and the proton conductivity can be described by a prefactor (A). This factor, in combination with the activation energy (E_a, eV) for the conduction, controls the ionic mobility in an Arrhenius relation according to:

$$\sigma_{H+} = A\exp\frac{-E_a}{RT}$$ Equation 6

From A it is possible to determine the effective carrier concentration and the E_a can be directly related to the system's structure. Typical values of the activation energy for perovskite systems ~0.4 – 0.5 eV[75], but even higher values for Ga-doped $BaZrO_3$[76] have been noted (0.72 eV). The higher E_a agrees well with the results from the quantum related calculations obtained by Björketun *et al.*[14] (0.59 – 0.62 eV). Ca- substituted $La_2Zr_2O_7$ have shown to have intermediate results (0.6 - 0.68 eV).[39] In papers I – V the E_a for the pyrochlore oxides are ~0.5 – 1 eV[77].

A non-linear Arrhenius plot can be seen for several oxide systems, due to the decrease of proton concentration and increase of the mobility with increasing temperature. At temperatures high enough for the proton conductivity to stop (~500 °C), oxide ion or electronic hole conduction may take place causing a linear Arrhenius behaviour[78,79].

3.6 Incorporation of protons

To successfully incorporate protons in a material, oxygen vacancies are needed. The samples can then be subjected to water vapour at elevated temperatures (Paper I-V). The water gas is taken up into the structure due to the dissociation of the water molecule into a hydroxyl group and a proton. The hydroxyl group fills an empty oxygen site and the proton forms a covalent bond with an oxygen in the structure. This can be described by the Kröger-Vink notation as follows:

$$H_2O(g) + O_O^{\,x} + V_O^{\bullet\bullet} \leftrightarrow 2OH_O^{\bullet}$$ Equation 7

The reaction is in general exothermic causing equilibrium to occur between the protons and the water vapour at low temperatures. Equilibrium occurs in the same manner between the oxygen vacancies and the water vapour at high temperatures. If the atmosphere is oxidising, a formation of electronic holes will follow due to the need to compensate for the oxygen vacancies according to:

$$^1/_2\, O_2 + V_O^{\bullet\bullet} \leftrightarrow O_O^{\,X} + 2h^{\bullet}$$ Equation 8

Both these reactions compete with the proton uptake. At low oxygen partial pressures, reduction can also occur via[80,81]:

$$O_O^{\,X} \leftrightarrow {}^1/_2\, O_2 + V_O^{\bullet\bullet} + 2\acute{e}$$ Equation 9

3.7 Proton concentration

In theory, the degree of protonation is equal to that of the acceptor doping concentration given that the valency of the dopant is one unit of charge. Hence, the chemical formula for 10% B-site Y-doped $La_2Zr_2O_7$ gives $La_2Zr_{1.8}Y_{0.2}O_{6.9}(O_{0.1}H_{0.2})$ assuming that all oxygen vacancies turn into protonic defects. Full hydration i.e. full protonic concentration, is seldom obtained regardless of

elevated time for hydration at perfect conditions, where several explanations for the problem have been given. Kreuer and Munch have suggested that a lower symmetry for the perovskite system linked to the reduced degree of hydration. The many site possibilities for the oxygen vacancy to occur at and hence a complexity of the process arises[82].

If the acceptor dopant is concentrated in the grain boundaries, the oxygen vacancy formation will be favoured here. This leaves the bulk with less possible sites for the protonation to occur and may cause a reduced proton concentration to a lowered theoretical hydration level[83].

Further, the doping of the B-site may not fully be directed here and some of the dopant may reside on the A-site instead. This further decreases the number of vacant oxygen sites, lowering the proton concentration in the sample[84].

3.8 Proton transport

The surplus of protons in an acceptor doped pyrochlore structure may relocate by a transferring step between the oxygen atoms. The action can be described as a reorientation and then a translation step of the hydrogen ion, i.e. the Grotthuss mechanism (Figure 9). It is still undecided which of the steps is rate-determining. Several experimental[85] and molecular dynamic[86] studies have been conducted on perovskite systems pointing at the reorientation step being the fastest. Other studies[87] show indications of strong hydrogen bonding from infrared (IR) result, equivalent to a faster proton transfer than reorientation step. This can be argued since the reorientation includes a breakage and a formation of hydrogen bonds[88].

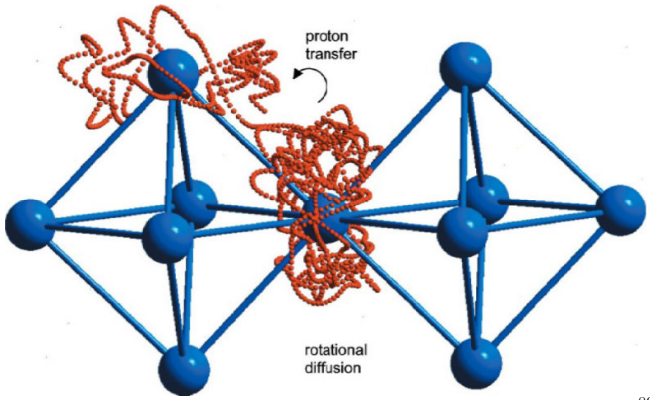

Figure 9. Grotthuss type proton transport mechanism. [89]

The proton motion may also be depend on the electronegativity of the B-site ion (Paper V). In theory, if the electronegativity is high, the electron density will be low on the oxygen ions in the octahedra. This will hence lower the strength of the interaction between the oxygen ion and the proton involved in the rotation and then transfer step. If the O-H interaction is weaker, the O-H bond should become longer. Therefore it might be expected to take less energy for the bond to break and the protons to move, when the ions on the B-site have higher electronegativity.

4 Experimental

4.1 Sample preparation

Depending on thermodynamic stability of the compounds and choice of synthesis route, crystalline solids can be prepared as ceramics, films, powders, nano-particles and single crystals[90]. Traditionally, the solid state method has been used to fabricate powders and polycrystalline materials. Compared to the other techniques its main flaw is the high temperature needed, typically T > 1000 °C. By mechanically alloying (milling) or using the sol-gel method, temperatures for the sintering step can be significantly reduced. However, finding the exact conditions for a sol-gel reaction is often hard and time consuming. Further, hydrothermal methods, intercalation/de-intercalation processes, vapour phase transport and thin film methods can also be used to synthesize crystalline solids.

In this section, the traditional solid state and the Pechini or sol-gel methods as well as the precursor route will be explained and discussed. The main results for the work have been carried out by high temperature solid state synthesis, due to the simplicity of the method and the accessibility of experimental equipment. However, both of the other methods have been tried to reduce synthesis time or decrease temperatures.

4.1.1 The solid state sintering method

The method is based on high temperature synthesis where the reactants are heated after mixing. The reaction rate is determined by kinetics and thermodynamics such as diffusion velocity and contact area of the crystallites. The temperature needs to be sufficiently high for the reaction to occur, which should generally be close to one of the reactants melting point.

The reactants are normally powders of metal oxides or carbonates (Eq. 10), which are mechanically milled or hand grinded, since they are inhomogeneous on atomic level. To enhance the surface of contact between the particles, the powders are pressed into pellets and then heated. The pellets are reground between every heating step since this will in theory increase the homogeneity of the resulting powder.

Example of reaction:

$$0.98La_2O_3(s) + 0.04CaCO_3(s) + 2SnO_2(s) \rightarrow (La_{1.96}Ca_{0.04})Sn_2O_{6.98}(s) + 0.04CO_2(g)$$

Equation 10

The first heating temperature must be high enough to enable evaporation of for instance carbonates (>900 °C). However, typical literature temperatures [91] for successfully achieving pure phased pyrochlores are in general higher (1400 – 1600 °C). Also the times for the sintering step are extensive (24 – 50 h) since the reaction is slow.

4.1.2 The Pechini, sol-gel or wet chemical route

The Pechini[92] or the sol-gel[93], also known as the wet chemical route is a description of a dissolution reaction by producing a gel (Eq. 11).

$$La_2O_3(s) + 1.5ZrO(NO_3)_2 \cdot 2H_2O + 0.25Y_2O_3(s) \rightarrow La_2Zr_{1.5}Y_{0.5}O_{6.75} \qquad \text{Equation 11}$$

The gel is composed by an alkoxide or an organic acid in combination with an alcohol, which polymerizes into easily dissolvable metals and a network of long chains. To increase the solubility of the system, for instance nitric acid can be added. The solution is gradually evaporated at lower temperatures (~200 °C). The solution ideally goes from a viscous solution with particles of colloidal dimensions to a transparent homogenous amorphous solid i.e. a gel. The gel is then continuously heated until a powder forms, which is pressed into a pellet and heated at higher temperatures (~1000 °C). The obtained powder will then typically have smaller crystallites, which is appropriate for thin films or fibres[94].

4.1.3 The precursor route

The precursor route is similar to the solid state synthesis. The reactants form an intermediate constituent, to facilitate formation of a pure phase product. The pre-phases are then reacted with another constituent, but at lower temperatures (Eq. 12).

$$0.8ZrO_2 + 0.1Y_2O_3 \rightarrow Zr_{0.8}Y_{0.2}O_{1.9}$$

$$La_2O_3 + 2Zr_{0.8}Y_{0.2}O_{1.9} \rightarrow La_2Zr_{1.6}Y_{0.4}O_{6.8} \qquad \text{Equation 12}$$

Here, the reactants in the first step were grinded, heated (1400 °C, 10 h) and re-grinded. The product ($Zr_{0.8}Y_{0.2}O_{1.9}$) was then mixed with La_2O_3, grinded, pelletized, heated (1500 °C, 50 h) and grinded. The gain by this method compared to the solid state and the sol-gel methods is hence time, due to the shorter initial heating (10 versus 24 h). However, pure phases were not readily obtained for the pyrochlore systems in this study and the compound had to go through an additional step of high temperature sintering.

4.2 Post-synthesis treatment

4.2.1.Vacuum drying

Drying of as-prepared samples was carried out in a conventional tube furnace set-up attached to a vacuum pump equipment (900°C, ~10 mbar, 8h). To ensure no uptake of protons from the surrounding, the samples were immediately transferred to a controlled environment.

4.2.2 Hydration and Deuteration

Structural proton uptake occurs at around 300 °C where powders or pellets were heated at different temperatures (300 - 500 °C, 120 h) under a flow of saturated gas. The samples were then examined via IR spectroscopy and TGA. Based on results regarding successful proton incorporation and mass loss, the samples were pressed into pellets and annealed for diffraction and spectroscopy as well as impedance studies. A flow (10 – 50 ml/min) of N_2 was bubbled through heated (76.2 °C) water or heavy water (D_2O) in a set-up according to Figure 10 below.

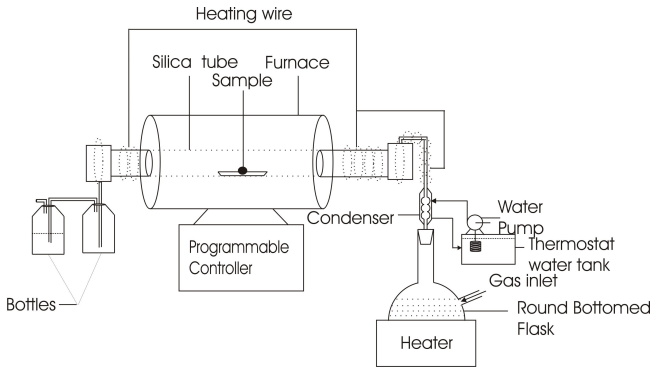

Figure 10. Hydration and deuteration set up.[95]

4.3 Characterization

4.3.1 Diffraction

To characterize the compounds, the initial tool of investigation used has been diffraction. Each crystalline compound has a unique diffraction pattern which arises from the compound's crystal lattices. To describe the crystal it can be divided into unit cells i.e. the smallest unit which is representative for the material. The unit cell is described by unit cell parameters which are three vectors (a, b, c). The positions of the atoms in the unit cell are given as lengths of the vectors with fractional coordinates (x, y, z).

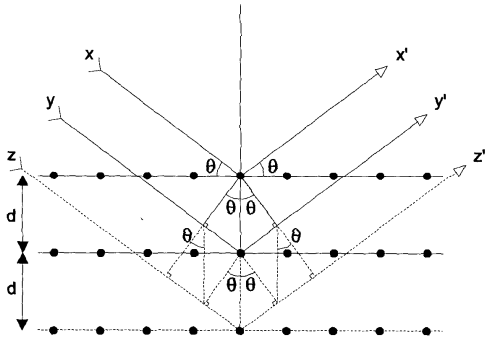

Figure 11. Schematic over constructive interference with incoming (x, y and z) and outgoing beams (x', y' and z'). [96]

If the path difference ($2d\sin\theta$) is an integer of the wavelength according to Equation 13, constructive interference will occur.

$$2d_{hkl}\sin\theta = n\lambda \qquad \text{Equation 13}$$

4.3.1.1 X-ray powder diffraction (XRD)

The diffraction patterns obtained for a sample are characteristic and unique fingerprints and the analytical technique in itself is non-destructive, quick, relatively cheap and simple for determining phase purity, degree of crystallinity and cell parameters. For the work related to this thesis, XRD was used for determination of unit cell parameters and phase purity. The studies were conducted on a Siemens D5000 diffractometer (Cu ($K_{\alpha1}$ +$K_{\alpha2}$) with an energy dispersive Sol-X^{TM} detector and a Bruker-AXS D8 Advance, with monochromated Cu $K_{\alpha1}$ radiation detected by a LynxEye^{TM} detector. For initial indexing, the program CellRef3[97] was used.

4.3.1.2 Neutron powder diffraction (NPD)

In neutron diffraction, a pulsed spallation source or a nuclear reactor is used. Examples of such facilities in Europe which use these types of neutron sources are ISIS at the Rutherford Appleton Laboratory, the U. K., and Institute Laue-Langevin (ILL), France.

Neutron diffraction is especially interesting due to its detection ability for light elements (H, O, N), when the signal from the same elements in XRD is hard to detect. Although both are diffraction techniques, the X-rays interact with electrons and neutrons with the nucleus. When a signal is generated from XRD, all photons from all electrons of the atom are scattered, which weakens the signal from lighter elements with few electrons. Neutron scattering however, is dependent on the isotropic scattering length (b) which randomly varies with atomic number. Moreover, here it is possible to separate adjacent atoms in the periodic table as well as isotopes of the same element from each other[98] such as H or D.

In this work the high neutron absorption of naturally occurring Sm, has precluded the use of NPD. A separate study looking for the deuteron site in $La_2Zr_{2-x}Y_xO_{7-\delta}$ systems is in progress.

4.3.2 Rietveld analysis

The Rietveld method[99] of analysis is based on computer modelling of whole powder diffraction patterns, with least-square structure refinement is used to fit the calculated patterns with the observed ones. In this study, the Rietveld refinement packages GSAS[100] was used, with an initial structural model taken from the literature.

4.3.3 Thermogravimetric analysis (TGA)

TGA analyses the change in mass of a compound as a function of time or temperature. An example of the result can be seen in Figure 12 (Paper II), where a continuous record of the mass change is displayed and the results are used for quantitative assessment of proton concentration.

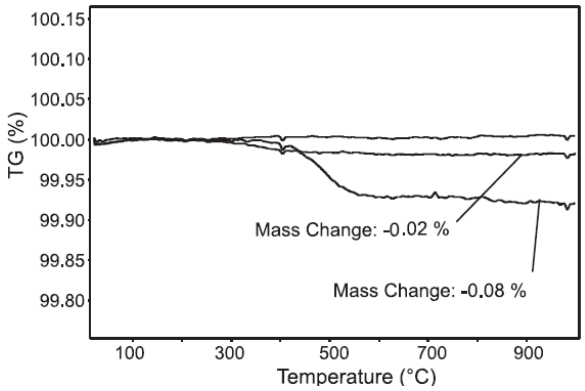

Figure 12. Mass change in $Sm_2Sn_2O_{7-\delta}$ pyrochlores.[101]

In addition, the endo- and exothermic heat flows can be recorded via differential thermal analysis (DTA) or differential scanning caliometry (DSC).

The NETZSCH™ STA 409 PC set up has a furnace with a thermocouple coupled to a balance. An unfilled reference and a filled (50 – 150 mg) sample pan (alumina or platinum crucibles) were placed on the scales. A safety gas (e.g. N_2) is run through the system (10 – 20 ml/min) and the chamber was evacuated twice before filling it with the carrier gas. A correction file was first recorded with the sample crucible empty, where the differences between the experimental and the correction file gives the sample mass loss.

For the work in this thesis, data has been collected mainly upon heating prehydrated samples, to determine the mass loss and the temperature at which it occurs. The temperature has been an indicator of which species has left the material and the aim was to detect mass loss in the 300 – 400 °C region where protons are expected to leave the material.

4.3.4 Infrared spectroscopy (IR)

The technique is originally denoted 'infrared' due to the fact that vibrational modes in matter can be excited by absorption of photons in the infrared (IR) region of the electromagnetic spectrum (10 – 13000 cm^{-1}). In particular the transitions involving the creation of a single quantum of vibration by absorption of a single photon are confined to the far IR (FIR:10-400 cm^{-1}) and middle IR (MIR:400-4000 cm^{-1}), while absorption of a single photon involving the creation of two or more vibrational quanta extends into the near IR (NIR: 4000-13000 cm^{-1}) and above. The IR technique is based on measuring the frequency dependence of the transmission through the sample or of the reflection off the sample of IR light. The magnitude of the absorption is directly related with the efficiency of reassigning the photon energy to the vibration of atoms in the sample[102] which depends on the change of the electric dipole moment caused by the vibration. Large changes are associated to strong absorption peaks and bands (Fig. 13).

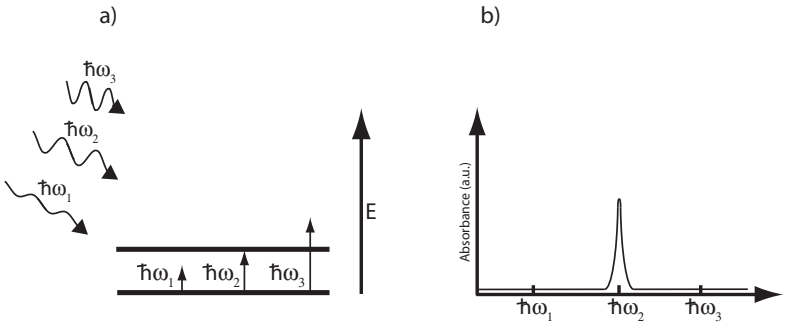

Figure 13. Absorption peaks and bands.[103]

The initial IR spectra were collected using a Nicolet Magna-IR 560 equipped with a KBr beam splitter, a deuterated triglycerine sulfate (DTGS) detector (400 - 4000 cm^{-1}) and an insert cell for diffuse reflectance spectroscopy. Individual and sharp peaks are reported on being typical features for hydrated pyrochlores which is reminiscent of those recorded for hydroxides, while is much different from typical spectra generally seen for acceptor doped perovskites[104]. The latter is due to the very many non-equivalent proton sites within the perovskites, since there are a vast numbers of local dopant induced distortions and hydrogen bonding. Previous research by Omata *et al.*[39] shows various IR spectra for Ca-doped $La_2Zr_2O_7$ where three bands are assigned to $La_{1.96}Ca_{0.04}Zr_2O_{7-\delta}$, showing two intense bands at 3517 and 3401 cm^{-1} indicating the presence of two distinct proton sites.

The compartment of the spectrometer is continuously purged with dry CO_2-free air. The diffuse reflectance technique was utilized, in which the incident beam was allowed to be reflected off the ground sample towards an overhead mirror upon which the diffusely scattered rays were collected by the detector. The absorbance spectra (64 scans/sample, resolution: 2.0 cm^{-1}) was an average value by taking the logarithm of the ratio between the reference (wrinkled aluminium foil) and the sample spectrum. The set up was monitored by and the data evaluated in the OMNIC E. S. P. program.

For further investigations at room and elevated temperatures, a Bruker IFS 66v/S vacuum Fourier Transform (FT) IR interferometer was used with a KBr beam splitter and a Mercury Cadmium Tellurium (MCT) detector (560 – 6000 cm^{-1}). The system was flushed with dry CO_2-free air. A diffuse reflection unit, model Praying Mantis, equipped with a small furnace was used in this case. The program OPUS was used to control the instrument and collect the data. A reference spectrum diffused from ground KBr was measured before collecting each sample (400 scans/run).

4.3.5 Scanning electron microscopy (SEM)

The morphology and microstructure of the samples were characterized with SEMs, where the technique is based on high resolution images formed from electrons[105]. A beam of electrons is passed through a series of magnetic lenses, which will end up focusing the beam and then bombards the sample. An interaction between the electrons from the beam and the electrons from the specimen occurs. This results in elastic collisions (electron-nucleus) giving backscattered electrons (BSE) and information on topography and composition or in-elastic (electron-electron) collisions providing energy to release e.g. secondary electrons (SE) giving information on morphology. The latter was the most important data for determining the morphology of the samples in this study.

Characterisation of the microstructure was carried out using a Leo Ultra 55 SEG SEM, operated with a typical acceleration potential of 2.5 kV and secondary electron (SE) detector.

4.3.6 Electrochemical impedance spectroscopy (EIS)

To characterise the electrical properties of a material, EIS was used, where a known single frequency voltage or current is applied to the sample via electrodes, and the response current or voltage is observed. It is assumed that the properties of the sample and electrodes are time invariant. The impedance is determined directly from the phase shift and amplitude at that frequency. This will result in an imaginary and a real part of the current. Typically, a single signal (Eq. 14) is applied to the cell and the resulting steady state current (Eq. 15) is measured[106].

$$\nu(t) = V_m \sin(\omega t) \qquad \text{Equation 14}$$

$$i(t) = I_m \sin(\omega t + \theta) \qquad \text{Equation 15}$$

Here, the $\nu(t)$ and the $i(t)$ are the voltage and current functions respectively, V_m and I_m are the voltage and the current amplitudes, ω is the angular frequency of rotation, t is the time and θ is the phase difference between the voltage and the current.

The impedance and its magnitude can be defined as follows (Eq. 16 and 17 respectively):

$$Z(\omega) = \nu(t)/i(t) \qquad \text{Equation 16}$$

$$|Z(\omega)| = V_m/I_m\ (\omega) \qquad \text{Equation 17}$$

The phase angle is defined as $\theta(\omega)$ and therefore the impedance (Z) will be a complex quantity, which becomes real only if $\theta = 0$ (for a pure resistor). It can be rewritten as (Eq. 18) using the conventional representation of complex numbers:

$$Z(\omega) = Z' + jZ'' \qquad \text{Equation 18}$$

From the vector representation below (Fig. 14), common geometry gives expressions for the real and imaginary part of the impedance (Eq. 19, 20, 21 and 22 respectively).

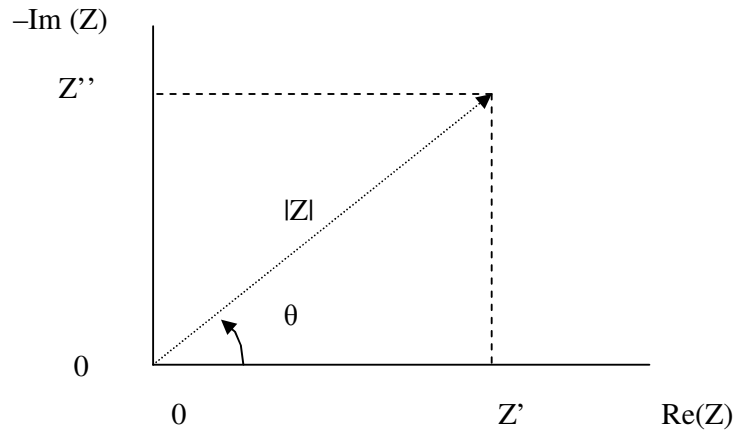

Figure 14. Vector representation of the real and imaginary part of impedance.[106]

$$\mathrm{Re}\,(Z) \equiv Z' = |Z|\cos\theta \qquad \text{Equation 19}$$

$$\mathrm{Im}\,(Z) \equiv Z'' = |Z|\sin\theta \qquad \text{Equation 20}$$

$$\theta = \tan^{-1}(Z'/Z'') \qquad \text{Equation 21}$$

$$|Z| = [(Z')^2+(Z'')^2]^{1/2} \qquad \text{Equation 22}$$

4.3.6.1 Single atmosphere experiments

The impedance was measured between 4.5 MHz and 1 Hz with a Solatron 1260 frequency response analyser, in a conductivity cell (ProboStat™; Norwegian Electro Ceramics AS, (NorECs).[107]

The sine wave amplitude was 1 V rms and to ensure good contact, around 0.8 cm^2 (Optic Zeiss 120 HD Microscope) of the pellets' surface were painted with conducting Pt-paste. Pt-grids were attached to the electrodes with Pt-wires. The pellet densities were ~ 80 % of the theoretical density and the measurement sequence was set to start with heating from room temperature up to 1000 °C under a flow of the desired measurement gas. The equilibrium time was set to 30 minutes and data collected on cooling in 50 °C intervals down to 150 °C. The data were collected on the same pellet under dry (Ar or O_2 flowed over two beds of the drying agent P_2O_5) and wet gas (Ar or O_2 bubbled through a H_2O or D_2O at room temperature). Two protective silica tubes were used to house the conductivity cell during the dry runs to ensure that any possible water uptake was minimised. For the wet runs a porous alumina (AL23) outer tube was used.

4.3.6.2 Double atmosphere experiment

The pellet was lightly polished, had a thickness of ~2 mm and a densitiy of 90% (Paper IV). The EIS was measured (4.5 MHz - 1 Hz) with a Hioki 3532-50 LCR HiTESTER. The surface of the pellet was painted with Pt-paste (~0.5 cm^2) and the data was collected upon cooling (500 – 300 °C) in 50 °C interval steps (30 - 60 min equilibrium time) under a flow of gas (100 – 1% O_2/O_2+H_2O/H_2+H_2O in N_2).

4.3.6.3 Data evaluation

When the impedance data of a system is represented as an equivalent circuit, the bulk properties should be denoted as a capacitor (C; geometrical capacitance) and an ohmic resistor (R) in parallel. In such case, the shape of the impedance feature is a perfect semi-circle.

However, in a typical ceramic sample there will be dispersion effects due to grain thickness and orientation of the grain boundaries. In addition, the signal from grain boundaries and the electrodes will have different time constants than those of the bulk and therefore several sets of RC or RQ elements can be placed in series to represent the true response of the material. The dispersion will influence the time constants so that a geometrical depression can be seen in the complex plane plots (Fig. 15) or a non-unity slope in the Bode plot (Fig. 16).

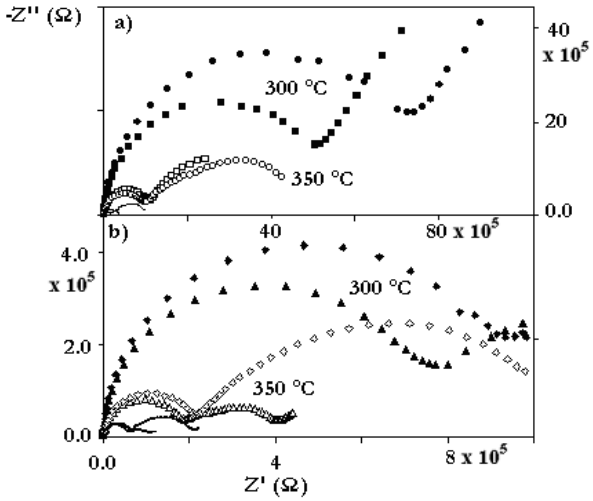

Figure 15. A complex plane plot for $La_{1.96}Ca_{0.04}Sn_2O_{7-\delta}$ pyrochlores.[108]

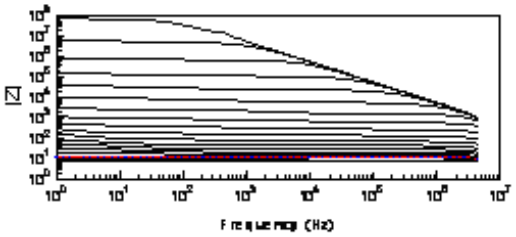

Figure 16. A Bode plot for $(Sm_{1.92}Ca_{0.08})Ti_2O_{6.96}$.[77]

To model this effect and the charge transfer effects at the electrode surfaces, a constant phase element (CPE) is often used instead of the pure C. A typical equivalent cirquit describing bulk, grain boundary and electrode signals can be seen in Figure 18 below[109].

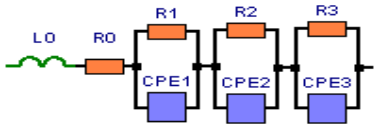

Figure 17. Schematics of an equivalent circuit.

Here the L_S is the correction for inductance (typically ~$1 \cdot 10^{-7}$ H; Paper IV). R1 and CPE1 are the resistor and constant phase element describing the bulk, while R2 and CPE2 are the same fitting the grain boundary. CPE3 refers to the electrode. In general all fitting of data should be thought of as empirical and therefore use as few elements for description as possible.

The fitting model for the data collected used was L(RQ)(RQ)Q (Paper IV) and typical values of how well the calculated model agreed with the measured data were χ^2 ~10^{-4}. In general, one to three time constants were observed in the impedance spectra. At high frequencies the time constant can be attributed to the bulk properties with a typical capacitance of 2-3 $\cdot 10^{-11}$ Fcm^{-2}.

For the studies with the simple gas set up (Paper I-III, V), the fitting and analysis were performed using the program ZView and for the controlled gas runs with ZSimpWin 3.21 from EChem Software. Both programs were based on using empirical equivalent circuits for evaluation.

4.3.7 Concentration cell method

AC conductivity measurements, such as EIS, give a wealth of information since the conductivity can be resolved into bulk and grain boundary contributions, and contributions from electrode reactions to the overall resistance can easily be determined due to their different time constants.
By measuring the conductivity of a material under varying oxygen and water vapour partial pressures and over a temperature range can yield valuable information about the defect chemistry of the material. By coupling it with the Electromotive Force (EMF) method in a concentration cell to determine transport numbers for oxide ions and protons under a similar set of conditions, a good understanding of total and partial conductivities is gained (Paper IV). This in turn determines whether the material is a good candidate for a particular application, under which conditions it can possibly find use, as well as guide efforts to improve its properties.

The EMF method is based on an open cell voltage measurement on a sample equipped with two reversible electrodes and subjected to a gradient in chemical potential. If small gradients are used, an average transport number can be assumed. The voltage measured over the sample will then be equal to

$$E_{EMF} = -\frac{RT}{nF} t_i \ln \frac{p_2}{p_1} \qquad \text{Equation 24}$$

where R, T, n and F are the universal gas constant, the temperature, the number of electrons transferred and Faraday's number, t_i is the average transport number and p_2 and p_1 are the partial pressures of the active species on either side of the sample.
Comparing this to the theoretical voltage calculated using the Nernst equation

$$E_{Nernst} = -\frac{RT}{nF} \ln \frac{p_2}{p_1} \qquad \text{Equation 25}$$

it is clear that the average transport number can be calculated by simply dividing the measured voltage with the calculated voltage.

$$t_{avg} = \frac{E_{EMF}}{E_{Nernst}} \qquad \text{Equation 26}$$

For systems where both oxide ionic and protonic conductivity is expected, the equilibrium between hydrogen, oxygen and water vapour must be taken into account, and the total voltage developed over the sample can be calculated as

$$E_{th} = \frac{RT}{4F}\left(t_O + t_H\right) \ln \frac{p_{O_2}^2}{p_{O_2}^1} - \frac{RT}{2F}\left(t_H\right) \ln \frac{p_{H_2O}^2}{p_{H_2O}^1}$$

or

$$E_{th} = \frac{RT}{2F}(t_O)\ln\frac{p^2_{H_2O}}{p^1_{H_2O}} - \frac{RT}{2F}(t_O + t_H)\ln\frac{p^2_{H_2}}{p^1_{H_2}}$$ Equation 27

For the EMF setup[110], the sample pellet was attached to platinum electrodes (Paper IV) and set onto the end of an alumina tube using a gold seal (Fig. 18)[111].

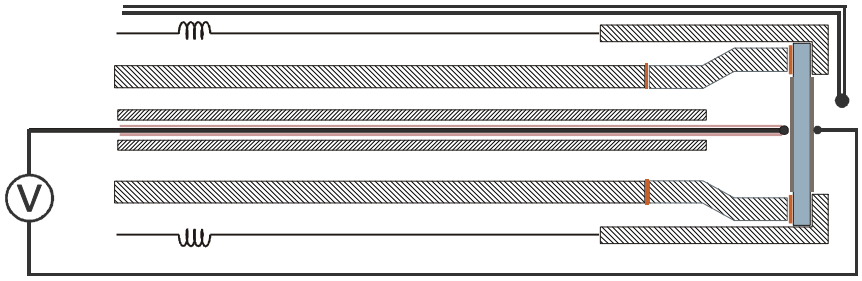

Figure 18. An EMF setup.[111]

Gas to the inner and outer compartments was supplied through stainless steel tubes from a gas mixer. The dry gas was bubbled through H_2O, and mixing the dry and wet gas enabled control of the water content of the gas. The experiments were carried out using the gas set up displayed in Table 2 with varying concentrations (100 – 10%).

Experimental configuration	Gas in outer compartment	Gas in inner compartment	Transport number determined
A	O_2	O_2/N_2	t_O
B	H_2O+O_2	H_2O/O_2	t_H
C	H_2O+H_2	H_2O+H_2/N_2	t_H

Table 2. Gas set up for Paper IV.

The water vapour concentration was measured using a *Dewlux* moisture meter with analog output, from MCM Ltd, Wetherby UK.. The temperatures were decreased from 500 °C to 300 °C in steps of 100 °C with varying equilibration times (30 min – 1h) depending on temperature and gas content.

4.3.7.1 Electrode polarization corrections

When conductivities in the intermediate temperature range are investigated using electrochemical concentration cell techniques, electrode polarisation resistance can lead to underestimation of ionic transport numbers. To correct for such problems, two known methods were carried out where the Liu and Hu correction is based on impedance measurements[112] at both gas extremes (10 and 100%). The other is a combination of impedance coupled with a variable load measurement[113], reported by Gorelov.

The Gorelov correction is expressed as:

$$\left(\frac{E_{th}}{E_{meas}}\right)-1=(R_i+R_\eta)\left(\frac{1}{R_e}\right)+\left(\frac{1}{R_b}\right) \qquad \text{Equation 28}$$

E_{th} = the thermodynamic EMF
E_{meas} = the measured EMF
R_i = the ionic resistance
R_η = the electrode polarization resistance
R_e = the sample's electronic resistance
R_b = the resistance caused by a resistance box coupled parallel to the electrodes

The Liu-Hu method is based on EIS data and concentrate on the effect of interfacial polarizations in species with known mixed conduction. The original expressions for the average ionic transference number (t_i) derived by Wagner[114] assumed infinite fast interfacial processes.

$$t_i=\frac{V_{OC}}{E_N} \qquad \text{Equation 29}$$

However, it has been found later that the interfacial resistances are the determining factors of the performance of particularly thin-film electrolytes. The average ionic and electronic resistances of the bulk electrolyte (R_i and R_e), the total resistance of the cell (R_T) and the resistance of the bulk electrolyte (R_b) can all be used to correct for the above. In combination with the open-cell voltage (V_{OC}) and the Nernst potential (E_N) a correction for the transport number expression can be derived according to:

$$t_i=\frac{R_e}{R_i+R_e}=1-\frac{R_b}{R_T}\left(\frac{1-V_{OC}}{E_N}\right) \qquad \text{Equation 30}$$

Paper IV had to rely mainly on the Gorelov-correction since the electrode resistance was hard to determine.

4.3.7.2 Electrode corrections

If the electrodes on the pellets do not cover the entire surface area of the pellet face, the calculated conductivity will only correspond to the cylinder defined by the electrodes. The part which is not covered in Pt-paste will also contribute to the conductivity of the material but is hence not included without the correction. This phenomenon can be denoted as fringing effects of the conduction through the material. Therefore, the conductivity was multiplied by a correction term for the electrodes (Paper IV). The values for the correction are calculated using finite element modelling.

5 Results and discussion

Papers I and II

5.1 A- and B-site substituted pyrochlores

The main motivation behind papers I and II was that there are extremely few studies relating to proton conduction of pyrochlores with transition metals other than zirconium at the B-site. Even though Shimura *et al.*[38] reported on $Y_2Ti_{1.8}M_{0.2}O_{7-\delta}$ Haugsrud and Norby studied $La_{1.98}Ca_{0.02}Ti_2O_{7-\delta}$[41] and Tuller *et al.*[115] studied the $Gd_2(Zr_xTi_{1-x})_2O_7$ system, the area is far from fully investigated

In papers I and II the synthesis and characterisation of four acceptor doped pyrochlores are presented, $(Sm_{1.92}Ca_{0.08})B_2O_{7-\delta}$, $Sm_2(B_{1.92}Y_{0.08})O_{7-\delta}$ (B = Ti, Sn) as well as the undoped $Sm_2Sn_2O_7$. The dopant ions and concentration were chosen to introduce the same nominal level of oxygen vacancies (δ = 0.04 for complete charge compensation) into the systems regardless of dopant site. The initial aim was for the results of the above systems to be part of a larger on-going study investigating the influence of different B-site metal ions and the influence of doping site on the proton conductivity of acceptor doped $Sm_2B_2O_7$ pyrochlores.

5.2 Structural aspects in XRD

To ensure phase purity and find cell parameters, XRD patterns were collected (Figure 19). Rietveld analysis revealed cell parameters of 10.5140(2), 10.5098(2) and 10.5158(2) Å for $Sm_{1.92}Ca_{0.08}Sn_2O_{7-\delta}$, $Sm_2Sn_{1.92}Y_{0.08}O_{7-\delta}$ and $Sm_2Sn_2O_7$ respectively.

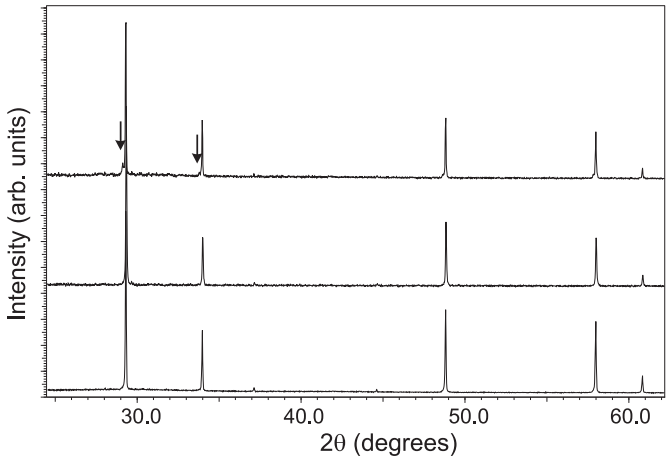

Figure 19. XRD patterns for $Sm_2Sn_{1.92}Y_{0.08}O_{7-\delta}$, $Sm_{1.92}Ca_{0.08}Sn_2O_{7-\delta}$ and $Sm_2Sn_2O_7$ from top to bottom respectively. Arrows mark the presence of an apparently cubic additional phase in the $Sm_2Sn_{1.92}Y_{0.08}O_{7-\delta}$ sample.

The ionic radii of the dopant ions are larger than the Sm^{3+} and Sn^{4+} ions that they are expected to replace and an expansion of the systems was expected. When refining the cell parameters, however, no such results were found for the acceptor-doped samples in comparison to $Sm_2Sn_2O_7$.

Recently, the structural and bonding properties of stannate pyrochlores were investigated using density functional theory.[116] When Sm^{3+} is set on the A-site, much stronger Ln-O_{48f} interactions will occur compared to other lanthanide cations. Further, the covalency of the Sn-O_{48f} bonds are higher than the Ln-O_{48f} and is also more covalent compared to other B-site pyrochlore oxides[117]. Hence, doping will cause a change in the size of the unit cell but may thereby influence the covalency and strength of the bonds. This can further lead to unexpected changes in the cell parameters. Alternatively, structural relaxation around the doped oxygen vacancies may outweigh the expected expansion of the unit cells.

Rietveld analysis allowed cell parameters of 10.246(1) and 10.238(1) Å to be determined for $Sm_{1.92}Ca_{0.08}Ti_2O_{7-\delta}$ and $Sm_2Ti_{1.92}Y_{0.08}O_{7-\delta}$ respectively which was expected.[118]

The presence of dissolved protons in the materials was indicated by the IR and TGA results, which show significant amounts of dissolved protons in the doped materials. The IR spectra for the undoped and A- and B-site doped Sn-systems are displayed in Figure 20.

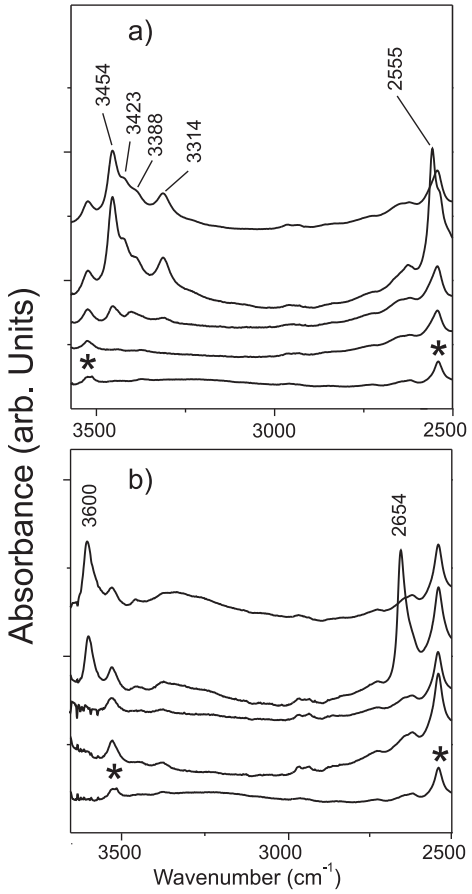

Figure 20. Infrared absorbance spectra of $Sm_{1.92}Ca_{0.08}Sn_2O_{7-\delta}$ (a) and $Sm_2Sn_{1.92}Y_{0.08}O_{7-\delta}$ (b). The spectra from top to bottom are of hydrated, deuterated, as-prepared and vacuum dried samples. The scan of as-prepared $Sm_2Sn_2O_7$ is also included at the bottom of both figures.

Comparing the A-site doped spectra with the B-site substituted sample, several peaks are seen in the 3500 cm^{-1} region for the first. This region is indicative of O-H stretch vibrations of structurally dissolved protons. Several peaks can suggest many possible stable sites for the protons to reside.

5.3 EIS

Enhancements of the bulk conductivity at temperatures up to 500-550 °C (Ti- and Sn-systems respectively) were observed for wet conditions. Proton conduction was confirmed by measurements in O_2/D_2O and Ar/D_2O (Figure 21).

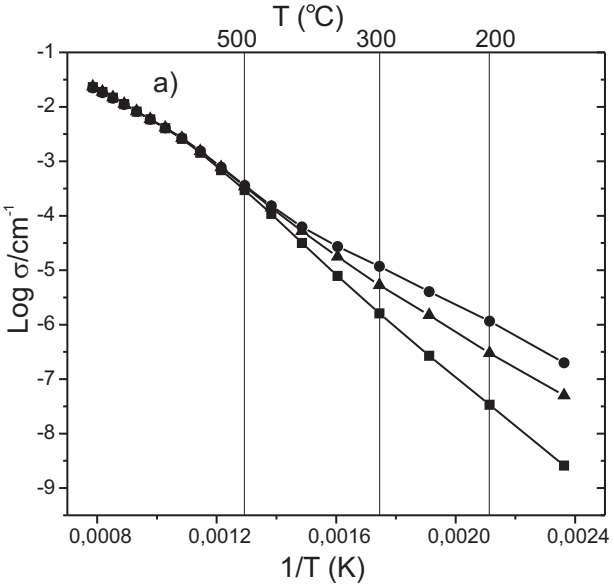

Figure 21. Arrhenius plots of the bulk conductivity of $Sm_{1.92}Ca_{0.08}Ti_2O_{7-\delta}$ where circles represent runs under $Ar+H_2O$, triangle $Ar+D_2O$ and squares dry Ar.

The results further reveal the importance of the correct choice of dopant site for the pyrochlore structure. For all systems, the A-site substitution yielded the highest levels of proton conduction. The $Sm_{1.92}Ca_{0.08}Sn_2O_{7-\delta}$ compound displayed mixed ionic and electronic conduction under dry oxidising conditions. The bulk proton conductivity at 300 °C gave 2.6 and 1 μScm^{-1} in H_2O-saturated Ar and O_2, respectively. The conductivity of $Sm_2Sn_{1.92}Y_{0.08}O_{7-\delta}$ and undoped $Sm_2Sn_2O_7$ generally was noted at about two orders of magnitude lower than for the A-site doped sample. Electron hole conduction dominated in dry atmospheres for $Sm_2Sn_{1.92}Y_{0.08}O_{7-\delta}$ and $Sm_2Sn_2O_7$.

The support for proton conduction in the undoped sample according to the dry and wet gas runs as well as the apparent isotope effect (Figure 22) is not expected due to the absence of dopants. This can possibly be explained by intrinsic anti-site defects creating oxygen vacancies at the 8*b* site.[101] The vacancy may arise if Sm^{3+} does not only dwell on the A-site, but also on the B- or Sn^{4+}-site, which could give the material a possibility to absorb and hence conduct protons. However, the IR and TGA results do not indicate any protons present in the material, which may be explained by the possibly very low levels of Sm^{3+} on the Sn^{4+} site.

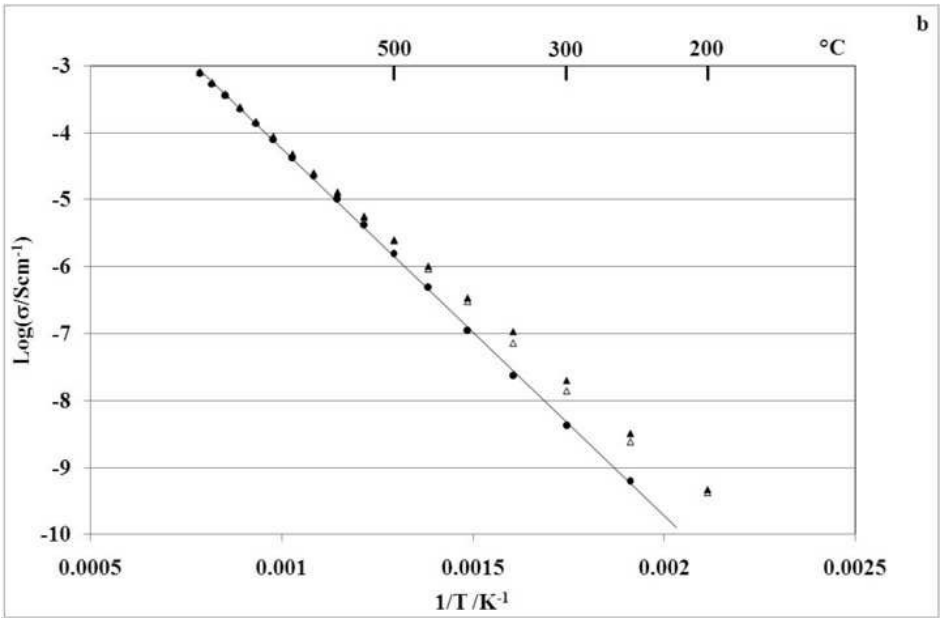

Figure 22. Arrhenius plots of the bulk conductivity of $Sm_2Sn_2O_7$ under O_2 (b) where dry gas corresponds to circles, D_2O are open triangles and H_2O filled triangles.

The Ti-based samples showed bulk, rather than grain boundary, conduction to be dominant as well as oxide ion conduction. For the A-site doped Sn-sample, bulk and grain boundary conduction could be separated. The Sn-based systems showed low levels of bulk proton conduction and high grain boundary impedance. Analysis according to the brick layer model showed that the grain boundaries are highly distorted.

The trend for Sn-based systems to decompose in reducing atmospheres is an important factor which will likely exclude $Sm_2Sn_2O_7$ derivatives from any potential SOFC related applications.

Paper III

5.4 The Lanthanide contraction

The Lanthanide contraction (Section 3.2) is a phenomenon which causes the lanthanides to decrease with increasing atomic number due to the low shielding effect of the f-electrons. Studies reporting the effect of lanthanide size for oxide systems have previously been carried out by Norby *et al.* [119] and Haugsrud and Norby [120]. A range of Ca-doped rare-earth niobate series, $RE_{1-x}Ca_xNbO_4$ (RE=La, Nd, Gd, Tb, Er, Y; x=0.01–0.05) showed dominating proton conductivities which decreased with decreasing radius of the rare-earth cations (La > Nd > Tb > Er). Generally the proton mobility and proton conductivity decreases with decreasing ion size and unit cell contraction. The reduction in mobility is explained by a more rigid lattice due to the decrease in polarizability of the proton-hosting oxide ion sublattice. Therefore, even if the oxygen ions are closer on average, the lattice is not as flexible and proton transfer becomes harder.
Tin-based systems were selected as the ionic radius of Sn unusually allows the stabilisation of the pyrochlore structure across the entire lanthanide series.[116] The focus of this paper was to

investigate the importance of the lanthanide ionic size compared with the proton conductivity in the $Ln_{1.96}Ca_{0..04}Sn_2O_{7-\delta}$ (Ln = La, Sm, Yb) pyrochlores.

XRD results clearly showed the effect of the lanthanide contraction, where the pattern of the La-containing material is shifted to lower 2θ-values, followed by the Sm-sample and finally the Yb-system (Figure 23).

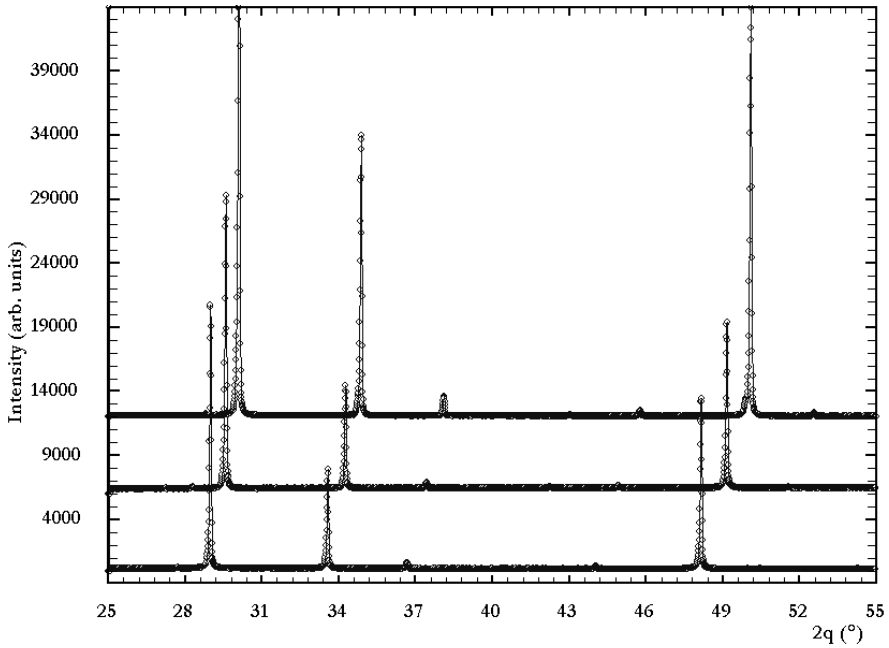

Figure 23. XRD patterns for $A_{1.96}Ca_{0.04}Sn_2O_{7-\delta}$ (A = La, Sm, Yb) from the bottom to the top pattern respectively.

The cell parameters determined from Rietveld analyses for the $(Ln_{1.96}Ca_{0.04})Sn_2O_{7-\delta}$ compounds were 10.7192(2), 10.5225(2) and 10.3182(3) Å for Ln = La, Sm and Yb respectively.

5.5 Structural aspects in IR

The IR spectra for the protonated (P), deuterated (D), as-prepared (AP) and vacuum dried (V) samples are shown in Figure 23. As expected, the hydrated and vacuum dried samples show the largest difference overall. For $La_{1.96}Ca_{0.04}Sn_2O_{7-\delta}$ (Figure 24a) the protonated and as-prepared samples are nearly identical suggesting protonation occurs from atmospheric humidity on cooling from the synthesis temperature. Three intense peaks can be seen at 3536 (α), 3496 (β) and 3251 (γ) cm^{-1}, along with at least two other bands. Protonated $Sm_{1.96}Ca_{0.04}Sn_2O_{7-\delta}$ (Figure 24b) reveals a similar spectra, with three intense bands at 3527, 3456 and 3311 cm^{-1} and two weaker peaks at 3422 and 3385 cm^{-1}.

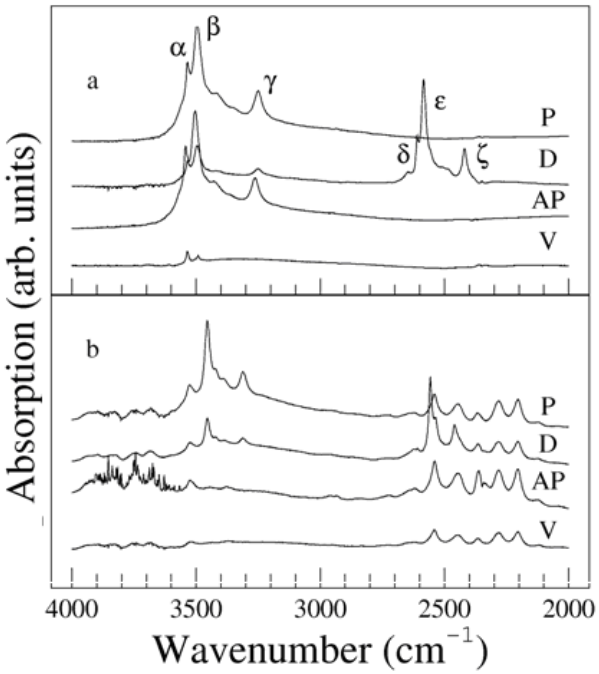

Figure 24. Infrared absorbance spectra for $A_{1.96}Ca_{0.04}Sn_2O_{7-\delta}$ (A = La, Sm; a and b respectively).

Both samples show clear isotope effects with strong intensities in the 2600 - 2400 cm^{-1} region (δ, ε and ζ for the La-sample. These peaks can be related to the O-H and O-D stretches through the expected ratio, i.e. $\upsilon_{OH} / \upsilon_{OD} \approx 1.37$.

All patterns for this lanthanide give the characteristic electronic f-f transitions for Sm (Figure 23b). When the Sm^{3+} ion is isolated all its f-electrons are degenerate, while in a crystal field several ion interactions must be taken into account. These can be seen as intraconfigurational transitions and will cause a splitting in the normally degenerate f-orbitals.
Transitions between the f-orbitals are normally 'spin-to-spin-forbidden' in a symmetric field. However, these compounds do not possess this type of symmetry and especially the rare-earth metals have levels where f-f-transitions can occur. Energetically such transitions will be seen in the IR-spectrum for Sm. One of the excited levels ($^6H_{9/2}$) can be seen as the five peaks in the 2555 – 2400 cm^{-1}region. The next excited level ($^6H_{11/2}$) can partly be seen in Figure 23b at 3600 cm^{-1} and above. The effect is denoted as a Stark effect (1919), which describes the splitting of spectral lines in an electrical field.

5.6 Proton conduction

The order of proton conductivity was found to be La ≈ Sm > Yb, confirming an influence of the the lanthanide size on the proton conductivity. $La_{1.96}Ca_{0.04}Sn_2O_{7-\delta}$ and $Sm_{1.96}Ca_{0.04}Sn_2O_{7-\delta}$ display similar levels of proton conductivity, whilst the conductivity of $Yb_{1.96}Ca_{0.04}Sn_2O_{7-\delta}$ lies well below these 2 samples. The data therefore indicates that higher levels of proton conductivity in pyrochlore systems is favoured for large and mid-sized lanthanides, and is dramatically less favourable for smaller lanthanides.

Paper IV

5.7 Combining EIS and EMF

To understand total and partial conductivities of a novel material is crucial to be able to determine what the material is a good candidate for. With EIS under varying oxygen and water vapour partial pressures over a temperature range, the defect chemistry of a compound can be modelled. EIS also give the possibility to separate the conductivity into bulk, grain boundary and electrode contributions. Combining defect chemistry with transport numbers for oxide ions and protons, obtained from the EMF technique under a similar set of conditions, a good understanding of the material can be obtained.

In this study, EIS connected to a controlled gas system was carried out on $Sm_{1.92}Ca_{0.08}Ti_2O_{6.96}$, where the results were compared to previously presented data from a simple gas supplied cell. Further, EMF measurements were carried out on the same system to find the transport numbers associated with the conduction processes.

5.8 Defect chemistry

The Kröger-Vink notation (Section 3.6) is used to describe the defect chemistry in this study and proton transport is likely to take place via the Grotthuss mechanism (Section 3.8). The dopant level determined the concentration of oxygen vacancies in these systems, which are replaced by protonic defects with increasing water vapour partial pressure. The EMF method (Section 4.3.7) is used to find the average transport number (t_{avg}) with the voltage measured over the sample (E_{EMF}) and the theoretical voltage (E_{Nernst}) according to:

$$t_{avg} = \frac{E_{EMF}}{E_{Nernst}}$$

This study is focused on intermediate temperatures (500 – 300 °C) under wet and dry gas ($H_2/N_2/O_2$). In these regions, electrode polarisation resistance may lead to underestimation of ionic transport numbers. To correct for such problems, two methods were looked at based on impedance measurements and variable load measurement (Section 4.3.7.1).

5.9 Transport numbers and conductivity

The total conductivity was dominated by bulk conductivity which was consistent with previous results (Paper I), and electronic conductivity appeared to play a slightly larger part in the grain boundaries. EMF confirmed the conductivity to be mainly ionic. At 300 and 400 °C the proton transport numbers were in agreement and the transport numbers for oxide ions was close to zero (Table 3). The protonic transport number was slightly lower in reducing conditions than in oxidising, indicating that some level of electronic conductivity was present.
At 500 °C the trend is the opposite, with the protonic transport number being close to zero, while the oxide ionic numbers are close to one.

			300 °C	400 °C	500 °C
t_O	High p_{O2}	Uncorrected	-	0	0.073
		Active load	-	0	0.986
		EIS	-	0	0.98
	Low p_{O2}	Uncorrected	-	-	0.75
		Active load	-	-	0.991
		EIS	-	-	0.98
t_H	High p_{O2}	Uncorrected	0.08	0.026	0
		Active load	1.06	0.947	0
		EIS	0.9	0.983	0
	Low p_{O2}	Uncorrected	0.42	0.34	0
		Active load	0.876	0.924	0
		EIS	1	0.935	0

Table 3. Overview of corrected and uncorrected values of transport numbers for 300 – 500 °C.

The clear difference between wet and dry conductivity measurements indicate proton conduction, which increase with decreasing temperature. The two curves for wet gasses are very similar, with the one obtained in oxygen being slightly higher in the high temperature region due to the inception of p-type electronic conductivity.

Paper V

5.10 Varying B-site ions

As mentioned for papers I and II, few studies have been carried out concerning proton conduction of pyrochlores with other transition metals than Zr at the B-site. Varying the B-site ion with increasing atomic number and ionic radii (Ti, (Sn), Zr, Ce) and investigate the effect on the proton conductivity was the primer motivation for the study. Finding additional trends in the electronegativity of the B-site ion, tolerance factors and proton incorporation, in light of proton conduction were further goals.

In combination with trying to map the area of varying the B-site constituent with proton conduction, $Sm_2Ce_2O_7$ derivatives were of interest due to their structure. These compounds have previously been investigated by Yamamura *et al.*[121] and found to exhibit a superstructure which was denoted the C-type phase (*Ia3*, Z = 32).

Moreover, pre-hydrated conductivity measurements were presented to further complete the study in terms of mobility and diffusivity.

5.11 Conductivity, mobility and diffusion

The diffusion coefficient (D) for the preprotonated $Sm_{1.92}Ca_{0.08}Sn_2O_{6.96}$ is more than one order of magnitude lower than for the Ti-structure (Figure 26) which is only slightly higher than the values obtained for distorted perovskites.[37] For the Zr- and Ce-structures the diffusion coefficient is more than 3 orders of magnitude lower compared to the Ti compound.

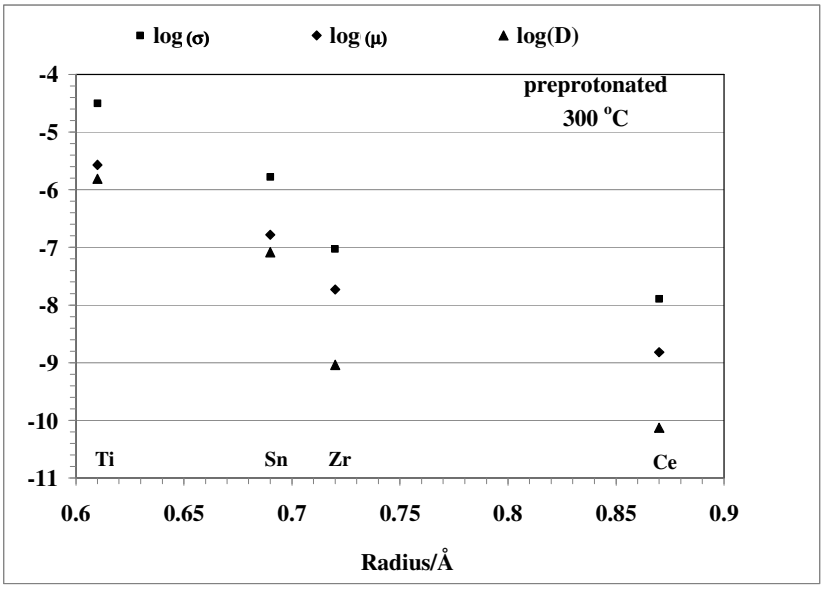

Figure 25. The diffusion coefficient D, mobility μ and the conductivity σ as a function of the ionic radius of the B-site ion.

These results show that a larger B-site ion makes the proton transfer more difficult. The calculated activation energy is also lower for the Ti-sample than for the Sn-sample showing the more facile transport of protons for the Ti-structure.

In the Ti-compound higher conduction in Ar, compared to oxygen, are seen. In the Sn-sample the trend is the opposite. This indicates that at high temperatures the Ti-sample is an predominantly an electron conductor, while the Sn material is a hole conductor.

6 Conclusions

The proton conductivity in acceptor doped pyrochlores $A_{2-x}Ca_xB_2O_{7-x/2}$ (A = La, Sm, Yb; B = Ti, Sn, Zr, Ce) and $A_2B_{2-x}Y_xO_{7-x/2}$ (A = Sm; B = Ti, Sn) have been investigated.

The $(Sm_{1.92}Ca_{0.08})B_2O_{7-\delta}$ and $Sm_2(B_{1.92}Y_{0.08})O_{7-\delta}$ (B = Ti, Sn) showed the presence of dissolved protons in the materials and proton conduction was confirmed by isotope effects. A trend of higher levels of proton conduction for A-site substituted pyrochlores in comparison to B-site doped systems was observed. The results show the importance of the correct choice of dopant site for the pyrochlore structure and are in accordance with previous findings on $La_2Zr_2O_7$ systems. The $Sm_{1.92}Ca_{0.08}Sn_2O_{7-\delta}$ compound displayed mixed ionic and electronic conduction under dry oxidising conditions. The Ti-based samples showed bulk, rather than grain boundary, conduction to be dominant as well as oxide ion conduction at higher temperatures.

The undoped $Sm_2Sn_2O_7$ system surprisingly showed an increase in conductivity under wet gas indicative of proton conduction. This effect may be explained by vacancies arising at the 8b site caused by some Sm^{3+} allocated at the Sn^{4+} site. The trend for Sn-based systems to decompose in reducing atmospheres is an important factor which will likely exclude $Sm_2Sn_2O_7$ derivatives from any potential SOFC related applications.

In the $Ln_{2-x}Ca_xB_2O_{7-x/2}$ (*Ln* = La, Sm, Yb) systems, the XRD results showed the effect of the lanthanide contraction. The order of proton conductivity was found to be La ≈ Sm > Yb, confirming a lanthanide dependence on the proton conductivity. The data therefore indicates that higher levels of proton conductivity in pyrochlore systems is favoured for large and mid-sized lanthanides, and is dramatically less favourable for smaller lanthanides.

The hydrated and deuterated samples show the largest difference in IR as well as isotope effects indicating presence. The many peaks suggest several possible proton sites in the structures. The Sm-sample also showed characteristic electronic f-f transitions known as the Stark effect (1919), which describes the splitting of spectral lines in an electrical field.

The transport numbers for $Sm_{1.92}Ca_{0.08}Ti_2O_{7-\delta}$ were confirmed by EMF to be mainly protonic at 300 and 400 °C. At 500 °C the protonic transport number was close to zero, while the oxide ionic numbers are close to one. In addition, the protonic transport number was slightly lower in reducing conditions than in oxidising, indicating that some level of electronic conductivity was present. Comparing wet and dry conductivity measurements, indicated proton conduction which increased with decreasing temperature.

Varying the B-site ion with increasing ionic radii in $Sm_{2-x}Ca_xB_2O_{7-x/2}$ (B = Ti, Sn, Zr, Ce) gave diffusion coefficient for the pre-protonated systems in the order of Ti > Sn > Zr > Ce. These results show that a larger B-site ion makes the proton transfer more difficult. The calculated activation energy was lowest for the Ti-sample.

Overall, $(Sm_{1.92}Ca_{0.08})B_2O_{6.96}$ (B = Ti and Sn) gave higher levels of proton conduction compared to the $(Sm_{1.92}Ca_{0.08})B_2O_{6.96}$ (B = Zr and Ce).

In general pyrochlores show some promise as proton conductors in the intermediate temperature region (200 – 600 °C). Several of the lanthanides have shown to form pyrochlore structures with B-site ions such as Sn^{4+}/ Nb^{5+}/Ta^{5+}/Ti^{4+}/Zr^{4+}, where the oxides are convenient to work with.

Most important, the Ti and Sn based pyrochlores have shown reasonably high proton mobilities. The lower levels of proton conductivities compared to known perovskite systems such as 10 % Y-doped $BaZrO_3$ and $BaCeO_3$, must be seen in the light of the low doping levels reported on in this study. By increasing the doping level, more vacancies can be formed, and the proton concentration and conductivity enhanced. This may also be true for systems where the ratio between the A- and the B-site is altered from the 1:1 relation.

However, introducing too high levels of doping or altering the A/B-site ratio excessively as well as using a dopant not suitable for the system, may cause phase impurities or distortions. This has further been seen to decrease the ion mobility in various systems as previously discussed. Therefore, the balance between possible proton incorporation and mobility is a delicate issue.

6.1 Future work

The research on various pyrochlore systems is still in progress where mixed conductivity in pyrochlore systems is of great interest. These systems have possible use in various parts of solid oxide proton fuel cells with the main direction towards electrolyte compounds and also as gas separation membranes.

Increasing the doping level to >10% for comparison to reported values for other systems in the literature, is a natural step in the further investigation. In addition, altering the A/B-site ratio and investigating the effect of various dopants, are further possible direction for research on these systems.

Further, the nature of the dopant could also play a large role for possible trapping effects as seen in perovskite structures. Therefore, by mapping various dopants such as Y^{3+}, In^{3+} and Sc^{3+}, proton conductivity may be increased.

Further investigations relating the microstructure with the conductivity is also of interest and a future post-doc project with focus on this issue would be beneficial for further understanding the pyrochlore systems.

7 Acknowledgements

I would like to thank Dr. Christopher Knee for his constructive and inspirational support in both experimental and theoretical studies. I would also like to thank my co-supervisor Prof Elisabet Ahlberg who has given me the great opportunity to be introduced to electrochemical impedance spectroscopy. I have learned a lot from both of you regarding research and leadership, which have been good lessons and I will keep this in mind for the future.

I am very thankful to my examiner Prof. David Turner who has provided me with the opportunity to be a PhD-student at the Chemistry Department at Gothenburg University. I have also come to know him to be a genuine support and a good person to talk to when it has been hard to see the path in front of me.

Without Prof. Sten Eriksson, several aspects of the laboratory work for this study would not have been possible and I am very thankful for the many suggestions he has given me regarding the practical aspects of this project.

I am also very grateful for the practical help and general support I have been given from my group members Dr. Annika Eriksson, Dr. Istaq Ahmed and Dr. Stefan Norberg, PhD-students Stefan Saxin, Habibur Raman and Francis Kinyanjui. My work has also been especially helped by the input from PhD-student Patrick Steegstra, Dr. Ezio Zangilini, Dr. Paul Henry and Prof. Vratislav Langer regarding SEM, IR, NPD and XRD analysis.

Senior researcher Nikos Bonanos has further given me the chance to visit with Risö National Laboratory, Denmark, where I have been able to explore both impedance spectroscopy and the electromotive force technique. There, I have had the chance to work with PhD-students Henrik Bentzer and Nicolai Bork and Dr. Sandrine Ricotte. Thank you so much for all the general support and I hope more good science to come.

I would also like to acknowledge the financial support from Vilhelm och Martina Lundgrens Vetenskapsfond, Stiftelsen Paul och Marie Berghaus Donationsfond, Jubileumsfonden, Adlerbertska Forskningsstiftelsen, Donationsstipendie, Gothenburg University, Knut och Alice Wallenbergs Stiftelse and SOAS Travel Grant. With help from these funds, my scientific work has been presented both nationally and internationally at conferences, workshops and meetings.

My special thanks goes to my mentor Ms. Birgitta Jönsson, who has been invaluable when it comes to giving other perspectives of various situations. I also want to express my gratitude to Dr. Å. Valadi who introduced me to the program Mentor4Research at Kungliga Ingenjörvetenskapsakademien, where I got to know Mr Claes Rydholm. All of you have played a big role in the preparations for a future carrier as well as giving lunch discussions a new dimension!

I am also very glad to have had the chance to get to know my fabulous female collegues Dr.:s Annika Eriksson and Hallgerd Eydahl as well as PhD-students Petra Rönnholm, Johanna Löberg, Jenny Perez-Holmberg, Liza Romero-Lejonthun and Linda Ingemarsson. Thank you so much for all the laughs, shoulders to lean on and positive support you have given me! You are all so bright and together I think we will have a smashing future!

Last I want to thank my family who is the reason I am here today. Thank you sister Maija Eurenius for all the fantastic pieces of advice throughout the years, especially the ones regarding chemistry. Without all of them I would have been lost! Also, thank you for always being there for me, not matter what the situation. I am truly proud to be your sister.
Thank you Uffe Dagnell for your impressive skills when teaching me about natural science and golf. It has been bliss to have you there through all the years!
Godfather Bengt Almström, you have always given me a roof over my head when in Stockholm, long conversations filled with pointers on life in general and many giggles. Thank you for being there and doing it so well for 28 years + all the ones to come.
I would also like to thank my mother and father in law, Jeanette and Hans Möller, for letting me sit in Onsala writing away when it has been hard to concentrate at home. Also, thank you all in the Möller-clan, for letting me feel so welcome in our new family!
A special acknowledgement also goes out to Ms. Dagmar Norberg and Mr. Tage Norgaard for always being so positive and enthusiastic about my sister, mother and I. You are fantastic!

This thesis is dedicated to the three people who have indirectly put a lot of work into the project. First, without my grand mother Gunvor Form's support I would not have grown up to the person I am today. Even though she is no longer with us, she has helped every day with her solid foundation of love that she has shown me since I was a child.

Second, I also owe this thesis to my mother Ingrid Eurenius, since she has never stopped believing in me. You have throughout been ever so happy when things have gone well, a great driving force when I have needed someone else to take over and a true listener when situations have turned bad. Further, thank you so much for walking me once a day when I was in my heaviest studying sessions! Also, thank you for all the food and cups of tea you have contributed with for this thesis. Most importantly, thank you for constant support. You are the best mother a daughter can ever have.

And third, is my husband Jonas Möller. Thank you for showing up in the rain and in the middle of the night with my samples that I had forgot. Thank you for sorting out me and my computer when both of us have been having nervous breakdowns. Thank you for not leaving me alone until you have seen a smile on my face. And thank you for presenting my research in your own words, the night before I had my talk in Glasgow. That was the most interesting view on proton conducting pyrochlores I think I will ever listen to in my entire life.
You have been with me through thick and thin and now we are in it for better or worse! It feels huge to embark on the adventure in Tokyo together, but I am not worried the least, since you will be with me. My heart, you and I made this day possible together.

8 References

[1]http://science.nasa.gov/headlines/y2003/images/fuelcell/sofc-brochure-new.gif
[2]K. D. Kreuer, Annu. Rev. Mater. Res. 33 (2003) 333
[3]H. Iwahara T. Esaka, H. Uchida and N. Maeda, Solid State Ionics 3/4 (1981) 359
[4]T. Scherban and A.S. Nowick, Solid State Ionics 35 (1989) 189
[5]R.C.T. Slade and N. Singh, Solid State Ionics 61 (1993) 111
[6]T. Omata, K. Okuda, S. Tsugimoto and S. Otsuka-Matsuo-Yao, Solid State Ionics 104 (1997) 249
[7]H. Iwahara, H. Uchida and S. Tanaka Solid state ionics, 9-10 (1983) 1021
[8]T. Norby and Y. Larring, Current Opinion in Solid State and Material Science, 2 (1997) 593
[9]J.A. Labrincha, J.R. Frade and F.M.B. Marques, Solid State Ionics 99 (1997) 33.
[10]T. Omata, M. Takagi and S. Otsuka-Yao-Matsuo, J. Electrochem. Soc. 150 (2003) E590.
[11]W. E. Klee, J. Inorganic Nucl. Chem. 31 (1969) 2367
[12]H. Yamamura, H. Nishino, K. Kakinuma and K. Nomura, Solid State Ionics, 178 (2007) 223
[13]S. Kramer and H. L. Tuller, Solid State Ionics 72 (1994) 59
[14]M. E. Björketun, C. S. Knee, B. J. Nyman and G. Wahnström, Solid State Ionics 178 (2008) 1642.
[15]T. Norby, Solid State Ionics, 125 (199) 1
[16]K.-D. Kreuer, Solid State Ionics 97 (1997) 1
[17]B. Gross, St. Marion, R. Hempelmann, D. Grambole, F. [40] T.O. Saetre, in: Proceedings of HYPOTHESIS II, Grimstad, Herrmann, Solid State Ionics 109 (1998) 13
[18]T. Norby, Nature 410 (2001) 877
[19]A. J. Appleby, Fuel Cell handbook, ISBN: 0-442-31926-6
[20]B. C. H. Steele, Nature, 414 (2001) 345
[21]http://americanhistory.si.edu/fuelcells/basics.htm
[22]T. Takahashi and H. Iwahara, Rev. Chim. Miner., 17 (1980) 243
[23]M. J. Scholten, J. Schoonman and J. C. van Miltenburg, Thermochim. Acta 268 (1995) 161
[24]K. D. Kreuer, Solid State Ionics, 149 (2000) 136
[25]M. S. Islam, P. R. Slater, J. R. Tolchard and Tim Dinges, Dalton Transactions 19 (2004) 3061
[26]H. Iwahara, T. Yajima, T. Hibino, K. Ozaki and H. Suzuki Solid State Ionics, 61 (1993) 65
[27]K. D. Kreuer, W. Münch, M. Ise, T. He, A. Fuchs, U. Traub and J. Maier, Ber. Bunsenges. Phys. Chem., 101 (1997) 1344
[28]M. E. Björketun, P. G. Sundell and Göran Wahnström, Physical Review B 76 (2007) 054307
[29]R. Haugsrud and T. Norby, Nature Materials 5 (2006) 193
[30]Y. Larring and T. Norby, Solid State Ionics 97 (1997) 523
[31]N. Kitamura, K. Amezawa, Y. Tomii and N. Yamamoto, Solid State Ionics, 163 (2003) 161
[32]E. Mollow, Zeitschrift fur Physik, 138 (1954) 487
[33]V. Rudolph, Z. Naturforsch, A13 (1958) 757
[34]Pope and Simkovich, Mat. R. Bull., 9 (1974) 1111
[35]T. Takahasi and H. Iwahara, Revue the Chimie Minerale 17 (1980)243
[36] H. Iwahara, H. Uchinda, K. Ono and K. Ogaki, Journal of the Electrochemical Society, 135 (1988) 529
[37]K. D. Kreuer, Solid State Ionics, 125 (1999) 285
[38]T. Shimura, M. Komori and H. Iwahara Solid State Ionics 86-88 (1996) 685
[39]T. Omata and S. Otsuka-Yao-Matsuo, J. Electrochem. Soc. 148 (2001) E252
[40]T. Omata, K. Ikeda, R. Tokashiki and S. Otsuka-Yao-Matsuo, Solid State Ionics 167 (2004) 389

[41]R. Haugsrud and T. Norby, Proceedings of the 26th Risø International Symposium on Materials Science: Solid State Electrochemistry (2005) 209.
[42]A. Petric and P. Huang, J. Mater. Cham. 5 (1995) 607
[43]H. Fjeld, R. Haugsrud, A. E. Gunnæs and T. Norby, Solid State Ionics 179 (2008) 1849
[44]T. Shimura S. Fujimoto, H. Iwahara, Solid State Ionics, 143 (2001) 117
[45]H. Yamamura, , H. Nishino, K. Kakinuma and K. Nomura, Solid State Ionics 158 (2003) 359
[46]R. Liu, Y. Xie, J. Wang, Z. Li and B. Wang Solid State Ionics 177 (2006) 73
[47]T. Norby Oddvar Dyrlie and Per Kofstad, Solid State Ionics 53-56 (1992) 446
[48]Y. Larring and T. Norby, Solid State Ionics 77 (1995) 147
[49]H. Yamamura, H. Nishino, K. Kakinuma and K. Nomura, J. Ceramic Society Japan, 111 (2003) 902
[50]O. Yokota, M. Yashima, N. Yamamoto and M. Yoshimura, J. Am. Ceram. Soc. 80 (9) (1997) 2429
[51]V. Grover S. N. Achary and A. K. Tyagi, J. Appl. Cryst. 36 (2003) 1082
[52]N. N. Greenwood and A. Earnshaw, The Chemistry of the Elements, ISBN-10: 0750628324
[53]D. F. Shriver and P. W. Atkins, Inorganic Chemistry; 3rd Edition, ISBN: 0-19-850331-8
[54]T. Norby, O. Dyrlie and P. Kofstad, The American Ceramic Soc. 75 (1992) 1176
[55]R. Haugsrud and T. Norby, Nature Materials 5 (2006) 193
[56]http://www.soton.ac.uk/~solids/pyrochlore.htm
[57]R. A. Chapman, D. B. Meadowcroft and A. J. Walkden, J. Phys. D: Appl. Phys. 3 (1970) 307
[58]Lev. Kantorovich, Quantum Theory of the Solid State: An Introduction; Volume 136, ISBN: 978-1-4020-2153-4
[59]R. C. Buchanan and T. Park, Materials Crystal Chemistry, ISBN: 0-8247-9798-1
[60]Elizabeth J. Harvey[a], Karl R. Whittle[a], Gregory R. Lumpkin[a], Ronald I. Smith[b] and Simon A.T. Redfern Journal of Solid State Chemistry, 178 (2005) 800
[61]K.V.G. Kutty, C.K. Mathews, T.N. Rao, U.V. Varadaraju , Solid State Ionics 80 (1995) 99
[62]J. Reading, C. S. Knee and M. T. Weller, J. Materials Chemistry 12 (2002) 2376
[63]A. Daidouh, C. Pico, M. L. Veiga, A. Almontassir, M. Abboudi and L. Hanebali, Solid State Sciences 6 (2004) 71
[64]A. Garbout, S. Bouattour, M. Ellouze and A.W. Kolsi, J. Alloys and Compounds 425 (2006) 88
[65]M Amarilla, M. L. Veiga, C. Pico, M. Gaitan and A. Jerez, Inorg. Chem. 28 (1989) 1701
[66]S. S. Kumar, K.V.O. Nair and J. James, J. Sol. State Chem. 177 (2004) 3873
[67]B. J. Kennedy, B. A. Hunter and C. J. Howard, J. Solid State Chemistry 130 (1997) 58
[68] A. V. Shlyakthina, A.V. Knotko, M.V. Boguslavskii, S.Yu. Stefanovich, I.V. Kolbanev, L.L. Larina and L.G. Shcherbakova, Solid State Ionics 179 (2008) 1004
[69]H.L. Tuller, Solid State Ionics 52, (1992) 135
[70]R. H. Mitchell, Perovskites: Modern and Ancient, ISBN: 0-9689411-0-9
[71]R. J. D. Tilley, Defect Crystal Chemistry and its Applications, ISBN: 0-412-01331-2
[72]T. Norby and P. Kofstad, Defects and Transport in Crystalline solids, Compendium for the advanced level course Defect Chemistry and Reactions in Solids, KJM 5120 and KJM 9120 (2007)
[73]J. P. Crocombette and A. Chartier, Nuclear Instruments and Methods in Physics Research B 250 (2006) 24
[74]R. J. D. Tilley, Defect crystal chemistry and its applications, ISBN: 0-412-01331-2
[75]K. D. Kreuer, Solid State Ionics, 125 (1999) 285
[76]I. Ahmed and E. Ahlberg, Advances of Solid Oxide Fuel cells II, Ceramic Engineering and Science Proceedings, 27 (2006) 105
[77]K.E.J. Eurenius, E. Ahlberg, I. Ahmed, S.G. Eriksson and C.S. Knee, Solid State Ionics doi:10.1016/j.ssi.2009.05.004

[78]T. Norby, M. Widerøe, R. Glöckner and Y. Larring, Dalton Transactions; Cambridge, the U. K. (2004) 3012
[79]J. F. Liu and A.S. Nowick, Solid State Ionics, 50 (1992) 131
[80]N. Bonanos, Solid State Ionics, 28-30 (1988) 579
[81]I. Kosacki and H. L. Tuller, Solid State Ionics, 80 (1995) 223
[82]W. Munch, K. D. Kreuer, S. T. Adams, G. Seifert and J. Maier, Phase Transitions, 68 (1999) 567
[83]F. Krug and T. Schober, J. American Ceramic Soc., 80 (1997) 794
[84]J. Wu, L. P. Li, W. T. P. Espinosa and S. M. Haile, J. Mat. Res., 19 (2004) 2366
[85]T. Matzke, U. Stimming, Ch. Karmonik, M. Soetratmo, R. Hempelmann and F. Giithoff, Solid State Ionics, 86-88 (1996) 621
[86]W. Munch, G. Seifert, K. D. Kreuer and J. Maier, Solid State Ionics, 97 (1997) 39
[87]M. Karlsson Mårten E. Björketun, Per G. Sundell, Aleksandar Matic, Göran Wahnström, Dennis Engberg and Lars Börjesson, Phys. Rev. B 72 (2005) 094303
[88]Qianfan Zhang, Göran Wahnström, Mårten E. Björketun, Shiwu Gao and Enge Wang Physical Review Letters 101, (2008) 215902
[89]W. Miinch, G. Seifert and K.D. Kreuer, J. Maier, Solid State Ionics 86-88 (1996) 647
[90]A. R. West, Solid State Chemistry and its Applications, ISBN: 0-471-90377-9
[91]M. Colombo, British ceramic Transactions, 98 (1999) 271
[92]M.P. Perchini, US patent 3330697 (1967)
[93]A. R West, Basic Solid State Chemisrty, ISBN: X
[94]M. Kakihana and M. Yoshimura, Bull. Chem. Jpn. 72 (1999) 1427
[95]I. Ahmed, PhD thesis, ISBN: 978-91-7385-101-5
[96]http://www.canberra.edu.au/irps/archives/vol13no2/Fig2.gif
[97]J. Laugier, http://www.ccp14.ac.uk/mirror/mirror.htm
[98]C. J. Howard and S. J. Kennedy, Materials Forum 18, (1994) 155
[99]H. M. Rietveld, J. Appl. Crystallogr., 2 (1969) 65
[100]A. C. Larsson et al, Los Alamos National Lab., Los Alamos (1994)
[101]K.E.J. Eurenius E. Ahlberg and C.S. Knee, Proton conductivity in $Sm_2Sn_2O_7$ pyrochlores, Submitted to Solid State Ionics (2009)
[102]D.L. Vien, N.B. Coltup, W.G. Fateley and J.G. Grasselli, Introduction to Infrared and Raman Spectroscopy, Academic Press Inc., 3rd Ed. ISBN-10: 012182554X
[103]M. Karlsson, PhD thesis, ISBN: 97891-7385-038-4, p.19
[104]I. Ahmed, S. G. Eriksson, E. Ahlberg, C. S. Knee, H. Götlind, L. G. Johansson, M, Karlsson, A. Matic and L. Börjesson, Solid State Ionics 178 (2007) 515
[105]B. L. Gabriel, SEM: A User's Manual for Materials Science, ISBN: 0-87170-202-9.
[106]E. Barsoukov and J. R. Macdonald, Impedance Spectroscopy: Theory, Experiment and Applications, 2nd Ed. ISBN: 0-471-64749-7
[107]www.norecs.com
[108]K.E.J. Eurenius E. Ahlberg and C.S. Knee, Proton conductivity in $Ln_{1.96}Ca_{0.04}Sn_2O_{7-\delta}$ (Ln = La, Sm, Yb) pyrochlores as a function of lanthanide size, Submitted to Solid State Ionics (2009)
[109]P. Agarawal, M. E. Orazem, L. H. Garcia-Rubio, Electrochemical Impedance spectroscopy, ISBN: 978-0-470-04140-6
[110]W. Plieth, Electrochemistry for Materials Science, ISBN: 978-0-444-52792-9
[111]H. Betzer, N. Bonanos, J. Phair 'EMF measurements on mixed protonic/electronic conductors for hydrogen membrane applications' , article in press, (2008).
[112] M. Liu and H. Hu, J. Electrochem. Soc., 143; 6 (1996) L109
[113] V. P. Gorelov, Inst. Of Electrochemistry Urals Science Center, 24 ;10 (1988) 1272
[114]C. Wagner, Z. Phys. Chem., B21 (1933) 25
[115]H.L. Tuller, Solid State Ionics 52, 135 (1992).

[116]Z. J. Chen, H. Y. Xiao, X. T. Zu, L. M. Wang, F. Gao, J. Lian and R. C. Ewing, Comp. Mater. Sci., 42 (2008) 653
[117]C. Jiang, C. R. Stanek, K. E. Sickafus and B. P. Uberuaga, Phys. Rev. B79 (2009) 104203.
[118]R.D. Shannon, Acta Crystallogr. A32 (1976) 751.
[119] T. Norby, O. Dyrlie, P. Kofstad, The American Ceramic Soc. 75 (1992) 1176
[120] R. Haugsrud, T. Norby, Nature Materials 5 (2006) 193
[121]H. Yamamura, H. Nishino, K. Kakinuma, K. Nomura, J. Ceramic Society Japan, 111 (2003) 902